

# CREDO: Epistemic-Aware Conformalized Credal Envelopes for Regression

Luben M. C. Cabezas<sup>1,2,4</sup>, Sabina J. Sloman<sup>3</sup>, Bruno M. Resende<sup>1</sup>, Fanyi Wu<sup>3</sup>, Michele Caprio<sup>3</sup>,  
and Rafael Izbicki<sup>1</sup>

<sup>1</sup>Department of Statistics, Federal University of São Carlos, São Carlos, Brazil

<sup>2</sup>Institute of Mathematics and Computer Science, University of São Paulo, São Carlos, Brazil

<sup>3</sup>The University of Manchester, UK, Department of Computer Science

<sup>4</sup>Université Grenoble Alpes, Inria, CNRS, Grenoble INP, LJK, France

March 10, 2026

## Abstract

Conformal prediction delivers prediction intervals with distribution-free coverage, but its intervals can look overconfident in regions where the model is extrapolating, because standard conformal scores do not explicitly represent epistemic uncertainty. Credal methods, by contrast, make epistemic effects visible by working with sets of plausible predictive distributions, but they are typically model-based and lack calibration guarantees. We introduce **CREDO**, a simple “credal-then-conformalize” recipe that combines both strengths. **CREDO** first builds an interpretable credal envelope that widens when local evidence is weak, then applies split conformal calibration on top of this envelope to guarantee marginal coverage without further assumptions. This separation of roles yields prediction intervals that are interpretable: their width can be decomposed into aleatoric noise, epistemic inflation, and a distribution-free calibration slack. We provide a fast implementation based on trimming extreme posterior predictive endpoints, prove validity, and show on benchmark regressions that **CREDO** maintains target coverage while improving sparsity adaptivity at competitive efficiency.

## 1 Introduction

Uncertainty quantification (UQ) has become a central requirement for modern machine learning systems, especially in settings where predictions inform downstream decisions. In regression, a central task is to construct prediction intervals for a future response  $Y_{n+1}$  at covariates  $X_{n+1} = x$ . Two complementary lines of work address this goal: conformal prediction (CP) provides distribution-free calibration, while imprecise-probability (credal) methods represent epistemic uncertainty via sets of plausible distributions but are typically model-based. In this paper, we combine these strengths to obtain prediction intervals that are both calibrated and epistemically interpretable.

On the calibration side, CP has emerged as one of the most influential approaches to distribution-free predictive inference because it offers distribution-free marginal coverage while assuming very little about the data-generating mechanism [Vovk et al., 2005, Shafer and Vovk, 2008, Lei et al., 2018]. In its split form, conformal inference is simple and scalable: one fits any predictive model on a training set, computes a nonconformity score on a calibration set, and then enlarges a model-based prediction set by a data-driven correction chosen to ensure coverage. However, standard conformal scores do not explicitly reflect *epistemic* uncertainty—uncertainty due to limited information—as opposed to *aleatoric* noise inherent in the data-generating process (see Section 1.2 for related work). As a result, split-conformal intervals can remain relatively narrow in regions of low local support where the underlying predictor extrapolates confidently; while marginal coverage is still guaranteed, the interval geometry may fail to communicate where predictions are driven by extrapolation rather than evidence.

From a different direction, the literature on imprecise probabilities and credal sets provides a principled language for epistemic uncertainty by representing beliefs not by a single distribution, but by a set of plausible distributions. Imprecise Probability (IP) theory [Walley, 1991, Augustin et al., 2014, Troffaes and de Cooman, 2014] studies uncertainty in how stochasticity is modeled. Credal sets, convex and (weak\*-)closed sets of probabilities [Levi, 1980], are among the main tools from IP theory. They are attractive precisely because they can make epistemic effects explicit: in poorly informed regions the set of plausible conditionals can widen, while additional evidence

can reduce this imprecision [Seidenfeld and Wasserman, 1993, Caprio and Seidenfeld, 2023]. Yet, credal prediction sets are typically *model-based* and thus *uncalibrated*: they depend on how the credal set is constructed and do not usually come with distribution-free coverage guarantees.

This paper aims to combine the best of both worlds in regression. We develop a framework that (a) produces interpretable credal predictive uncertainty to represent local epistemic effects, and (b) retains the distribution-free marginal coverage guarantee of conformal calibration. Concretely, we start from a local credal set of conditional predictive distributions  $\mathcal{F}_0(x)$ , induce from it a *credal quantile envelope*  $[\ell(x), u(x)]$  that summarizes the range of plausible conditional quantiles, and then apply split conformal calibration using a distance-to-envelope score. The resulting prediction interval, CREDO (Conformalized Regression with Epistemic-aware creDal envelOpes), is easy to implement, retains distribution-free marginal coverage, and expands adaptively in regions where the credal envelope reflects limited local information.

Figure 1 illustrates the motivation on a toy regression with a structural transition near  $x = 0$  and weaker covariate support toward the extremes. Both CQR [Romano et al., 2019] and CREDO are split-conformal and thus target the same marginal coverage, but their *geometry* differs: CREDO selectively widens where local evidence is weak (near the transition and at the edges), whereas CQR can remain comparatively uniform and appear overconfident in sparse regions. CREDO also makes this behavior diagnosable via a decomposition of interval width into aleatoric and epistemic components, with epistemic uncertainty peaking exactly where the envelope inflates.

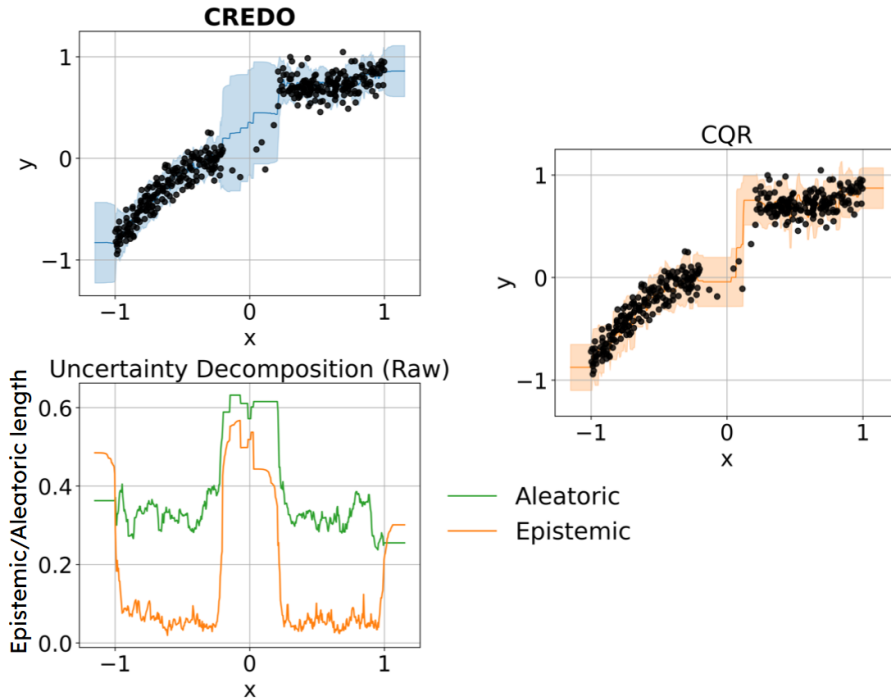


Figure 1: **Motivation and decomposition.** Comparison of split-conformal prediction intervals. *Top-left:* CREDO yields intervals that widen adaptively in regions of high epistemic uncertainty—near the transition and toward the covariate extremes. *Top-right:* CQR (which does not take epistemic uncertainty into account) produces comparatively uniform intervals that can look overconfident where local support is weak (few nearby training points), despite marginal validity. *Bottom-left:* CREDO enables an uncertainty decomposition into aleatoric (green) and epistemic (orange) components; epistemic uncertainty peaks around  $x = 0$  and at the edges, aligning with where CREDO inflates the envelope.

## 1.1 Novelty

Our contributions are:

**Credal-to-conformal regression via an explicit envelope.** We propose CREDO, which starts from a covariate-dependent credal set of predictive distributions  $\mathcal{F}_0(x)$  and summarizes it by a  $(1 - \alpha_0)$  credal quantile envelope

$[\ell(x), u(x)]$ . We then conformalize this envelope using a distance-to-envelope score, guaranteeing finite-sample marginal coverage under exchangeability.

**A lightweight credal construction from posterior endpoint trimming.** We introduce an endpoint-trimmed posterior credal set that produces envelopes by trimming extreme posterior predictive endpoints. This yields a simple and scalable mechanism to encode epistemic effects without modifying the conformal machinery.

**Diagnostics via a width decomposition.** We provide a practical diagnostic that attributes interval width to (i) an aleatoric core from the conditional model, (ii) an epistemic inflation term induced by credalization, and (iii) the conformal calibration slack. This makes it possible to localize *why* uncertainty is large at a given  $x$ .

## 1.2 Relation to Other Work

**Conformal Inference.** Conformal prediction yields distribution-free predictive sets by calibrating a nonconformity score  $s(x, y)$  on held-out data and inverting an empirical  $(1 - \alpha)$  quantile, guaranteeing finite-sample marginal coverage under exchangeability [Vovk et al., 2005, Shafer and Vovk, 2008, Papadopoulos et al., 2002, Lei et al., 2018, Angelopoulos and Bates, 2021, Cabezas et al., 2025b]. From the standpoint of epistemic uncertainty, this guarantee does not by itself ensure that sets expand in data-sparse or extrapolative regions: widely used regression scores (including residual scores and CQR-style quantile-distance scores) often track primarily aleatoric variability, so the resulting expansion can be weakly sensitive to lack of local support [Lei et al., 2018, Romano et al., 2019, Izbicki et al., 2020, 2022, Hüllermeier and Waegeman, 2021, Izbicki, 2025].

Motivated by this, a growing line of work augments conformal prediction with epistemic-aware scores so that the conformal expansion increases when the predictor is extrapolating. For example, Cochetoux et al. [2025] modifies weighted regression-split conformal prediction by redefining the scale term to represent epistemic uncertainty about  $Y$ , estimated via Monte Carlo dropout. Closest to our regression setting, Rossellini et al. [2024] propose uncertainty-aware CQR variants that inflate the CQR score using ensemble-based proxies for epistemic instability in the estimated quantiles (e.g., ensemble standard deviation in UACQR-S or ensemble order statistics in UACQR-P). A complementary, score-centric route is EPICScore which models the conditional distribution of a base score with Bayesian tools and then transforms the score to make epistemic effects visible while retaining conformal calibration [Cabezas et al., 2025c], though it can require large calibration samples to learn this conditional score distribution. While these methods successfully inject epistemic information into conformal calibration, the epistemic component typically enters as an implicit score-rescaling and is therefore harder to interpret. In contrast, CREDO yields calibrated intervals whose width admits a transparent decomposition into aleatoric noise, credal (epistemic) inflation, and calibration slack, enabling direct inspection of where each type of uncertainty grows.

**Bayesian Predictive Inference.** Bayesian predictive inference constructs uncertainty regions by integrating parameter uncertainty through the posterior distribution [Bernardo and Smith, 2009]. In this framework, uncertainty arises from both aleatoric variability and epistemic uncertainty about model parameters [Hüllermeier and Waegeman, 2021]. While posterior predictive intervals are calibrated under correct model specification, they may substantially under-cover under misspecification or distribution shift, since their validity depends on the assumed likelihood model [Jansen, 2013, Ovadia et al., 2019].

Several recent works combine Bayesian modeling with conformal prediction. For example, Fong and Holmes [2021] use posterior predictive densities as nonconformity scores, and Wu et al. [2026] optimize the conformal threshold under a decision-risk problem via Bayesian Quadrature. Bayesian-conformal hybrids also appear in the Gaussian-process literature, where GP posterior uncertainty is leveraged to widen calibrated sets away from observed inputs [Jaber et al., 2024, Pion and Vazquez, 2024]. Conformalized Bayesian Inference [Bariletto et al., 2025, Cabezas et al., 2025a] takes a different approach by applying conformal prediction directly to Bayesian posterior distributions in parameter space, yielding valid uncertainty regions for parameters and derived quantities. These approaches typically rely on a single posterior predictive distribution that averages over parameter uncertainty.

In contrast, our method encodes epistemic uncertainty through *credal sets* of predictive distributions. This representation captures not only parameter uncertainty but also model ambiguity, providing a principled way to inflate predictions when multiple modeling explanations are compatible with the local data. As a result, the induced inflation can be more robust in data-sparse or extrapolative regions, where a Bayesian posterior may extrapolate confidently due to inductive bias or approximation artifacts. We then conformalize the resulting ambiguity-aware envelopes, retaining finite-sample marginal coverage under exchangeability.

**Credal Sets and Imprecise Probabilities.** Rather than restricting to a single probability distribution, the theory of imprecise probabilities represents epistemic uncertainty by second order distributions, random sets, or credal sets [Walley, 1991]. In this paper, we focus on the latter for its ease of implementation and interpretation. Credal sets arise naturally when evidence is insufficient to uniquely identify a distribution, and provide a principled framework for separating epistemic from aleatoric uncertainty [Abellan et al., 2006, Hüllermeier and Waegeman, 2021]. Recent work has established formal connections between conformal prediction and imprecise probability. In particular, Cella and Martin [2022] show that, under a minimal assumption, conformal p-values induce an upper envelope  $\overline{P}(A) = \sup_{P \in \mathcal{P}} P(A)$ , for all measurable sets  $A$ , for a credal set  $\mathcal{P}$  of predictive distributions.

Building on this perspective, Caprio et al. [2025a], Caprio [2025] prove that a classical conformal prediction region coincides with the imprecise highest density regions (IHDR, the IP version of a credible interval) of the credal set  $\mathcal{P}$ , thereby revealing a structural equivalence between conformal prediction and certain imprecise probabilistic constructions. Recent work further explores this connection from an epistemic uncertainty perspective. Chau et al. [2026] show that split conformal prediction implicitly induces a predictive credal set, and propose a mutual-model-information criterion to quantify epistemic uncertainty within this framework. Relatedly, Caprio et al. [2025b] develop conformalized credal regions for classification with ambiguous ground truth, combining credal uncertainty with conformal validity guarantees. Similarly, Javanmardi et al. [2024] introduce conformalized credal set predictors that leverage conformal calibration to construct distributionally robust prediction sets while retaining finite-sample validity.

Rather than interpreting conformal regions as arising from an induced credal set, we explicitly construct a covariate-dependent credal set of predictive distributions to model local epistemic uncertainty, and subsequently apply split conformal calibration. In this way, CREDO integrates credal modeling and conformal validity at the level of predictive distributions.

## 2 Methods

Our goal is to construct prediction sets for a real-valued response  $Y_{n+1}$  given covariates  $X_{n+1} = x$  that (i) encode *local epistemic uncertainty* through a covariate-dependent *credal* set of predictive distributions, and (ii) enjoy *finite-sample, distribution-free marginal coverage* via conformal calibration. Let  $D = \{(X_1, Y_1), \dots, (X_n, Y_n)\}$  be an exchangeable dataset. We split  $D$  into a training set  $D_{\text{tr}}$  and a calibration set  $D_{\text{cal}}$  of size  $m := |D_{\text{cal}}|$ . All model-based quantities (credal sets and envelopes) are learned using  $D_{\text{tr}}$ ; the conformal correction is computed using  $D_{\text{cal}}$ .

**High-level idea.** Fix a “credal nominal” level  $\alpha_0 \in (0, 1)$  and a conformal level  $\alpha \in (0, 1)$ . For each covariate value  $x$ , we:

1. Construct a local credal set of conditional predictive distributions  $\mathcal{F}_0(x)$  for  $Y \mid X = x$ .
2. Take the credal *quantile envelope*  $[\ell(x), u(x)]$  induced by  $\mathcal{F}_0(x)$  at level  $1 - \alpha_0$ .
3. Use the distance-to-envelope score  $s(x, y)$  and compute its calibration quantile  $\hat{\tau}$  on  $D_{\text{cal}}$ .
4. Output the conformalized interval  $C(x) = [\ell(x) - \hat{\tau}, u(x) + \hat{\tau}]$ .

The final interval can be interpreted as an *aleatoric core* (from the conditional model), plus an *epistemic expansion* (from the credal set), plus a *distribution-free calibration expansion* (from conformal). Figure 2 summarizes our procedure. Next, we detail each of these steps.

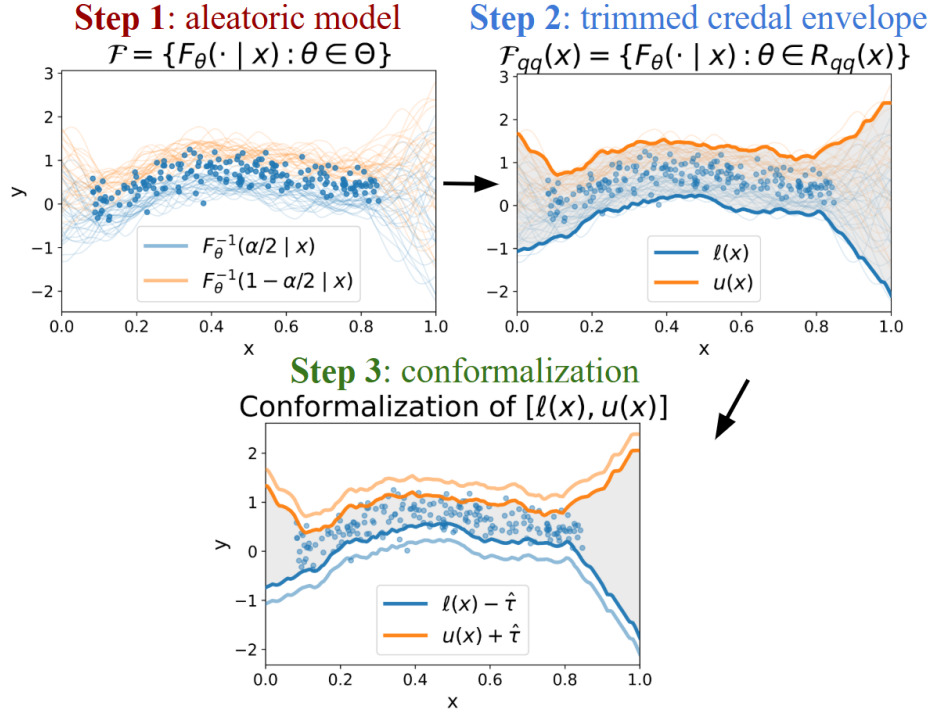


Figure 2: CREDO scheme. From a model for the aleatoric uncertainty, we form a trimmed credal quantile envelope  $[\ell(x), u(x)]$  (at nominal level  $1 - \alpha_0$ ), then split-conformalize using the distance-to-envelope score to output  $C(x) = [\ell(x) - \hat{\tau}, u(x) + \hat{\tau}]$  with marginal coverage  $1 - \alpha$ .

**Step 1: conditional aleatoric model and local credal sets.** We start from a (possibly nonparametric) conditional model class  $\mathcal{F} = \{F_\theta(\cdot | x) : \theta \in \Theta\}$ , where  $F_\theta(\cdot | x)$  denotes the conditional CDF of  $Y$  given  $X = x$ . The likelihood model  $F_\theta$  is assumed precise; epistemic uncertainty is represented through uncertainty about  $\theta$ . We define a local credal predictive set at covariate value  $x$  to be any subset  $\mathcal{F}_0(x) \subseteq \mathcal{F}$ , interpreted as the collection of predictive distributions deemed plausible at  $x$  after observing  $D_{\text{tr}}$ . In Section 2.1 we discuss how to choose  $\mathcal{F}_0(x)$  in this paper, although our framework is general.

**Step 2: credal quantile envelope.** Fix  $\alpha_0 \in (0, 1)$ . For each covariate value  $x$ , we define the credal envelope

$$[\ell(x), u(x)] = \left[ \inf_{F \in \mathcal{F}_0(x)} F^{-1}(\alpha_0/2 | x), \sup_{F \in \mathcal{F}_0(x)} F^{-1}(1 - \alpha_0/2 | x) \right]. \quad (1)$$

By construction, for every  $F \in \mathcal{F}_0(x)$ , the model-based central interval  $[F^{-1}(\alpha_0/2 | x), F^{-1}(1 - \alpha_0/2 | x)]$  is contained in  $[\ell(x), u(x)]$ .

*Remark 2.1.* The credal set  $\mathcal{F}_0(x)$  induces a predictive probability box (p-box, that can be thought of as an interval of CDF's) [Augustin et al., 2014, Section 4.6.4] via the lower/upper CDF bounds  $\underline{F}(t | x) := \inf_{F \in \mathcal{F}_0(x)} F(t | x)$  and  $\overline{F}(t | x) := \sup_{F \in \mathcal{F}_0(x)} F(t | x)$ . Using the generalized inverse  $G^{-1}(p | x) := \inf\{t : G(t | x) \geq p\}$ , the quantile envelope (1) depends only on this p-box, as  $\ell(x) = \overline{F}^{-1}(\alpha_0/2 | x)$  and  $u(x) = \underline{F}^{-1}(1 - \alpha_0/2 | x)$ .

**Steps 3–4: conformal calibration of the credal envelope.** The credal envelope  $[\ell(x), u(x)]$  is not guaranteed to be calibrated in finite samples. To obtain distribution-free validity, we apply split conformal calibration using the nonconformity score

$$s(x, y) := d(y, [\ell(x), u(x)]) = \max\{\ell(x) - y, y - u(x)\},$$

which measures how far  $y$  lies outside the credal envelope [Romano et al., 2019]. Let  $\hat{\tau}$  be the  $[(m + 1)(1 - \alpha)]$ -th order statistic of the calibration scores  $\{s(x_i, y_i) : (x_i, y_i) \in D_{\text{cal}}\}$ . The final prediction set at covariate value  $x$  is

$$C(x) = \{y : s(x, y) \leq \hat{\tau}\} = [\ell(x) - \hat{\tau}, u(x) + \hat{\tau}]. \quad (2)$$

## 2.1 One implementation of Step 1: endpoint-trimmed posterior credal sets

We now specify the choice of  $\mathcal{F}_0(x)$  used in the experiments in this paper. The key idea is to represent epistemic uncertainty by retaining only those posterior predictive distributions whose central predictive endpoints are not extreme under the posterior. This yields an interpretable and computationally light credal set.

In order to do that, we adopt a Bayesian perspective and place a prior  $\pi(\theta)$  on  $\Theta$ , leading to a posterior  $\pi(\theta | D_{\text{tr}})$ . Fix  $\alpha_0 \in (0, 1)$  and define the predictive endpoints under parameter value  $\theta$ :

$$\begin{aligned} q_L(\theta, x) &= F_\theta^{-1}(\alpha_0/2 | x) \text{ and} \\ q_U(\theta, x) &= F_\theta^{-1}(1 - \alpha_0/2 | x). \end{aligned}$$

Under  $\theta \sim \pi(\theta | D_{\text{tr}})$ , the pair  $(q_L(\theta, x), q_U(\theta, x))$  is random. Fix a trimming level  $\gamma \in (0, 1)$  and set  $C_L(x)$  and  $C_U(x)$  to satisfy

$$\begin{aligned} &\pi(q_L(\theta, x) \leq C_L(x) | x, D_{\text{tr}}) \\ &= \pi(q_U(\theta, x) \geq C_U(x) | x, D_{\text{tr}}) = \gamma/2. \end{aligned}$$

Intuitively, this discards the  $\gamma/2$  lowest lower endpoints and the  $\gamma/2$  highest upper endpoints under the posterior. We define the endpoint-trimmed parameter set as

$$R_{qq}(x) = \{\theta : q_L(\theta, x) \geq C_L(x), q_U(\theta, x) \leq C_U(x)\},$$

and the induced local credal set  $\mathcal{F}_{qq}(x) = \{F_\theta(\cdot | x) : \theta \in R_{qq}(x)\}$ . By the union bound, notice that the posterior probability of  $R_{qq}(x)$  is at least  $1 - \gamma$ . Finally, the credal envelope with respect to this credal set is the *trimmed endpoint envelope*

$$[\ell(x), u(x)] := [C_L(x), C_U(x)]. \quad (3)$$

This envelope is easy to implement via Monte Carlo and captures posterior endpoint dispersion in a way that is directly interpretable as epistemic uncertainty. Indeed, in practice, we draw  $\theta^{(1)}, \dots, \theta^{(B)} \sim \pi(\theta | D_{\text{tr}})$ , compute endpoint draws  $q_L^{(b)}(x), q_U^{(b)}(x)$ , and set  $C_L(x), C_U(x)$  to the empirical  $(\gamma/2)$ -quantile of  $\{q_L^{(b)}(x)\}_{b=1}^B$  and the empirical  $(1 - \gamma/2)$ -quantile of  $\{q_U^{(b)}(x)\}_{b=1}^B$ , respectively. Section A in the Appendix shows the full CREDO algorithm.

## 2.2 Data-Density-Aware Credal Sets

Posterior predictive intervals from common Bayesian learners can be too insensitive to local data scarcity, yielding overconfident sets in data-sparse regions unless epistemic structure is injected explicitly [Ovadia et al., 2019]. For instance, BART is built from regression trees with constant leaf values, hence its fits are piecewise constant in  $x$  [Chipman et al., 2010], and standard tree extrapolation can become flat outside the training range [Wang et al., 2022]. Furthermore, a global conformal correction may fail to adequately account for heteroscedasticity even in highly populated regions [Lei et al., 2018, Romano et al., 2019]. While a uniform shift  $\hat{\tau}$  might be necessary to cover concentrated aleatoric noise in some areas, applying the same slack to well-supported, low-noise regions leads to overly conservative intervals that ignore the model’s localized precision.

These limitations motivate using a covariate-dependent  $\gamma(x)$  that adapts to local information density. By replacing the fixed  $\gamma$  with  $\gamma(x)$ , we selectively retain more posterior mass—yielding wider credal envelopes—where covariate support is low and the model is prone to overconfidence. Conversely, in regions with high data density,  $\gamma(x)$  allows for thinner envelopes, leveraging localized precision to reflect greater confidence in the model’s estimates.

Concretely, for each  $x$ , we define  $C_L(x)$  and  $C_U(x)$  as before but with  $\gamma$  replaced by  $\gamma(x)$ . A smaller  $\gamma(x)$  retains more posterior realizations, typically yielding a wider envelope to capture epistemic uncertainty, whereas a larger  $\gamma(x)$  trims more aggressively to produce efficient, tight intervals in well-supported areas. Importantly, because  $\gamma(x)$  depends only on the covariates  $X$ , the split conformal validity of Equation (2) is preserved.

In our implementation, we choose  $\gamma(x)$  according to

$$\gamma(x) = \gamma_{\max} - (\gamma_{\max} - \gamma_{\min}) \sigma\left(\frac{\text{sc}(x) - m_\gamma}{\tau_\gamma}\right),$$

where  $\text{sc}(x)$  is a scarcity score,  $m_\gamma, \gamma_{\min}, \tau_\gamma$ , and  $\gamma_{\max}$  are constants and  $\sigma(x)$  is the logistic sigmoid function. The idea is that, if  $x$  is in a data-sparse region,  $\gamma(x)$  will be small (close to  $\gamma_{\min}$ ), leading to less trimming on the credal set construction (i.e., larger sets). On the other hand, in well-supported regions,  $\gamma(x) \approx \gamma_{\max}$ .

To construct the scarcity score, we start with  $\phi : \mathcal{X} \rightarrow \mathbb{R}^d$ , a representation in which Euclidean distances are meaningful (for tabular data,  $\phi(x)$  can be standardized covariates; for complex inputs, it can be a learned embedding [Wilson et al., 2016] from the predictive model). Fix  $k$  and, for any  $x$ , let  $X_{(k)}(x)$  denote the  $k$ -th nearest neighbor of  $x$  among the training covariates  $\{X_i : (X_i, Y_i) \in D_{\text{tr}}\}$ . Define the kNN radius  $r_k(x) := \|\phi(x) - \phi(X_{(k)}(x))\|$ , so larger  $r_k(x)$  indicates lower local design density around  $x$ . To make  $r_k(x)$  comparable across problems, we compute reference quantiles on the training set, e.g.  $q_{\text{lo}} = \text{Quantile}_{0.50}(\{r_k(X_i)\})$  and  $q_{\text{hi}} = \text{Quantile}_{0.95}(\{r_k(X_i)\})$ , and form the scarcity score

$$\text{sc}(x) := \frac{r_k(x) - q_{\text{lo}}}{q_{\text{hi}} - q_{\text{lo}} + \varepsilon}. \quad (4)$$

where  $\varepsilon > 0$  is small. We detail standard choices for each parameter and representations in Appendix C.2.

Figure 3 shows the data-support-aware trimming level  $\gamma(x)$  as a function of  $x$  in a toy example. In well-supported regions,  $\gamma(x)$  is larger, so more aggressive endpoint trimming keeps the credal envelope  $[\ell(x), u(x)]$  close to the baseline posterior interval. In data-sparse or extrapolative regions,  $\gamma(x)$  becomes smaller, reducing trimming and thereby widening  $[\ell(x), u(x)]$  to reflect increased epistemic uncertainty.

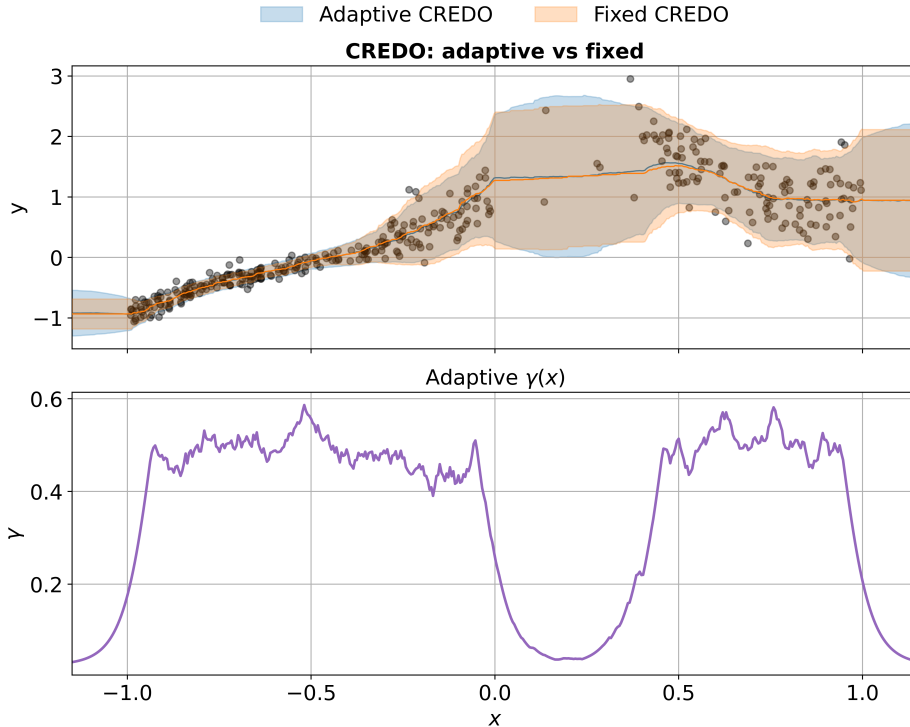


Figure 3: **Data-support-aware trimming via  $\gamma(x)$ .** *Top:* Prediction intervals under a constant trimming level  $\gamma$  versus the adaptive rule  $\gamma(x)$  driven by a kNN-based scarcity score. Adaptive trimming decreases  $\gamma(x)$  in data-sparse/extrapolative regions (less endpoint trimming, wider credal envelopes) and increases  $\gamma(x)$  in data-dense regions (more trimming, tighter envelopes). *Bottom:* The resulting  $\gamma(x)$  profile as a function of the covariate  $x$ .

### 2.3 Uncertainty Decomposition

A central feature of CREDO is that it yields an interpretable decomposition of the final conformal interval length into (i) an aleatoric baseline coming from the conditional model, (ii) an epistemic contribution induced by posterior uncertainty over predictive endpoints, and (iii) a distribution-free calibration adjustment.

For each parameter value  $\theta$ , we define the conditional (aleatoric) central interval at covariate  $x$ ,  $I_\theta(x) = [q_L(\theta, x), q_U(\theta, x)]$ , and its length  $|I_\theta(x)| = q_U(\theta, x) - q_L(\theta, x)$ . We summarize the irreducible (aleatoric) uncertainty at  $x$  by the posterior mean length

$$\begin{aligned} U_A(x) &:= \mathbb{E}[|I_\theta(x)| \mid x, D_{\text{tr}}] \\ &= \int (q_U(\theta, x) - q_L(\theta, x)) d\pi(\theta \mid D_{\text{tr}}). \end{aligned}$$

We then decompose the total length of  $C(x)$  (Eq. 2) as

$$|C(x)| = \underbrace{U_A(x)}_{\text{aleatoric baseline}} + \underbrace{\left( \left| [\ell(x), u(x)] \right| - U_A(x) \right)}_{\text{epistemic contribution}} + \underbrace{2\hat{\tau}}_{\text{distribution-free calibration slack}}.$$

In practice,  $U_A(x)$  is estimated via Monte Carlo draws  $\theta^{(1)}, \dots, \theta^{(B)} \sim \pi(\theta \mid D_{\text{tr}})$ :

$$\hat{U}_A(x) = \frac{1}{B} \sum_{b=1}^B (q_U(\theta^{(b)}, x) - q_L(\theta^{(b)}, x)),$$

while  $|\ell(x), u(x)|$  is obtained directly from the trimmed endpoint quantiles, and  $\hat{\tau}$  is computed from the calibration scores (2).

### 3 Theory

We begin by showing that the credal quantile envelope defined in Eq. 1 is conservative for every distribution in the local credal set. Concretely, for any fixed  $x$  and any  $F \in \mathcal{F}_0(x)$ , the credal envelope covers  $Y \mid X = x$  with probability at least  $1 - \alpha_0$  (according to  $F$ ):

**Theorem 3.1.** *Assume  $[\ell(x), u(x)]$  is defined by (1). Then for every fixed  $x$  and every  $F \in \mathcal{F}_0(x)$ ,*

$$\mathbb{P}_F(Y \in [\ell(x), u(x)] \mid X = x) \geq 1 - \alpha_0.$$

The next theorem provides a posterior-predictive lower bound on the coverage probability, showing that trimming at level  $\gamma$  yields a Bayesian predictive mass of at least  $(1 - \gamma)(1 - \alpha_0)$  inside the trimmed envelope. These results characterize the credal step as a principled (and interpretable) enlargement of a nominal conditional interval.

**Theorem 3.2.** *Fix  $x \in \mathcal{X}$  and consider the endpoint-trimmed construction in Section 2.1 at nominal level  $\alpha_0 \in (0, 1)$  and trimming level  $\gamma \in (0, 1)$ , with  $[\ell(x), u(x)] = [C_L(x), C_U(x)]$  as in Eq. (3). Define the (Bayesian) posterior predictive probability by*

$$\mathbb{P}(\cdot \mid X = x, D_{\text{tr}}) := \int \mathbb{P}_\theta(\cdot \mid X = x) d\pi(\theta \mid D_{\text{tr}}),$$

where  $\mathbb{P}_\theta(\cdot \mid X = x)$  denotes probability under the conditional model  $F_\theta(\cdot \mid x)$ . Then

$$\mathbb{P}(Y \in [\ell(x), u(x)] \mid X = x, D_{\text{tr}}) \geq (1 - \gamma)(1 - \alpha_0).$$

The credal envelope alone, however, is not guaranteed to be calibrated under any data-generating process. However, its conformalized, CREDO, version does achieve the correct marginal coverage:

**Theorem 3.3.** *Let  $(X_1, Y_1), \dots, (X_n, Y_n), (X_{n+1}, Y_{n+1})$  be exchangeable. Then the CREDO set  $C(X_{n+1}) = [\ell(X_{n+1}) - \hat{\tau}, u(X_{n+1}) + \hat{\tau}]$  satisfies the distribution-free guarantee*

$$\mathbb{P}(Y_{n+1} \in C(X_{n+1})) \geq 1 - \alpha.$$

Finally, under correct specification and posterior consistency, we show that this conformal correction is asymptotically benign: Theorem 3.4 proves that the trimmed envelope endpoints converge to the oracle conditional quantiles, the conformal expansion  $\hat{\tau}$  vanishes, and the conditional coverage converges to the nominal level. Together, these theorems justify CREDO as combining (i) explicit, covariate-dependent epistemic uncertainty through credal sets with (ii) finite-sample distribution-free validity through conformal calibration, while recovering the oracle interval asymptotically under standard Bayesian regularity.

**Theorem 3.4.** *Suppose Assumption D.2 holds (in particular,  $\alpha_0 = \alpha$ ). Construct the endpoint-trimmed envelope as in Section 2.1:  $[\ell(x), u(x)] = [C_L(x), C_U(x)]$ , where  $C_L(x)$  is the  $(\gamma(x)/2)$ -posterior quantile of  $q_L(\theta, x)$  and  $C_U(x)$  is the  $(1 - \gamma(x)/2)$ -posterior quantile of  $q_U(\theta, x)$ , and let  $C(x) = [\ell(x) - \hat{\tau}, u(x) + \hat{\tau}]$  be the CREDO interval. Then, as  $n_{\text{tr}} \rightarrow \infty$  and  $m \rightarrow \infty$ , for  $P_X$ -almost every  $x$ ,*

(i) *Envelope endpoints converge to the oracle endpoints:*

$$(\ell(x), u(x)) \xrightarrow{\mathbb{P}_{\theta^*}} (q_L^*(x), q_U^*(x)),$$

where  $q_L^*(x) = F_{\theta^*}^{-1}(\alpha/2 | x)$  and  $q_U^*(x) = F_{\theta^*}^{-1}(1 - \alpha/2 | x)$ .

(ii) *The conformal correction vanishes:*  $\hat{\tau} \xrightarrow{\mathbb{P}_{\theta^*}} 0$ .

(iii) *Conditional coverage converges to the nominal level:*

$$\mathbb{P}_{\theta^*}(Y \in C(x) | X = x, D_{\text{tr}}, D_{\text{cal}}) \xrightarrow{\mathbb{P}_{\theta^*}} 1 - \alpha.$$

## 4 Experiments

We evaluate CREDO across 12 standard regression benchmarks (see Appendix B for dataset details). Each experiment follows a randomized protocol, splitting the data into training (56%), calibration (24%), and test (20%) sets, with performance metrics averaged over 30 independent runs. All evaluated methods target a 90% marginal coverage level ( $\alpha = 0.1$ ). For CREDO, we initialize the credal level at  $\alpha_0 = \alpha$  and construct trimmed endpoint envelopes derived from posterior samples.

Our implementation uses a Bayesian Quantile Neural Network (QNN) backend, where we evaluate two primary variants: CREDO-QNN with a fixed credal level and an adaptive variant employing our covariate-dependent  $\gamma(x)$  scheme. Technical implementation details for both variants are provided in Appendix C. The remainder of this section is structured as follows: Section 4.1 provides a comparative analysis against state-of-the-art conformal prediction methods, focusing on conditional coverage efficiency and epistemic awareness. Subsequently, Section 4.2 validates the interpretability of CREDO by evaluating the behavior of our decomposed epistemic uncertainty across inliers and outliers.

### 4.1 Baseline comparisons

To evaluate CREDO, we compare it against the following state-of-the-art conformal quantile regressors: standard CQR and CQR-r [Romano et al., 2019, Sesia and Candès, 2020], the epistemic-aware UACQR-S and UACQR-P [Rossellini et al., 2024], and EPICScore [Cabezas et al., 2025c]. These baselines span from classical split conformal methods based on quantile regression to more recent approaches that explicitly incorporate epistemic. Further implementation details are provided in Appendix B.3.

Performance is assessed via two primary objectives: conditional coverage efficiency and adaptivity to model ambiguity. We measure the former using the Scaled Mean Interval Score (SMIS), which jointly penalizes interval width and miscoverage [Gneiting and Raftery, 2007] to serve as a proxy for the conditional coverage properties of the sets. To evaluate response to data scarcity, we report the Interval Length Ratio (ILR)—the ratio of mean interval lengths for test-set outliers relative to inliers [Cabezas et al., 2025c]. A higher ILR distinguishes methods that effectively inflate uncertainty in regions with low covariate support, reflecting a more sensitive capture of local epistemic signals. Extended results, metric definitions and outlier detection details are provided in Appendix B.

Across all benchmarks, both CREDO variants achieve the target 90% marginal coverage, confirming split-conformal validity in practice (Table 4, Appendix B.4). Regarding SMIS (Table 1), CREDO remains consistently competitive, often outperforming or statistically matching strong conformal baselines; specifically, the adaptive variant is a top performer in 9 out of 12 datasets.

CREDO also demonstrates superior outlier adaptivity. ILR results (Table 2) show that both variants consistently produce the highest ratios, indicating effective selective widening on atypical points without sacrificing global efficiency or coverage. This effect is most pronounced in small-data regimes, where increased posterior dispersion in sparse regions allows CREDO to better capture local epistemic uncertainty. Furthermore, CREDO maintains outlier coverage closer to nominal levels in the majority of scenarios (Table 5, Appendix B.4), further highlighting its enhanced epistemic awareness.

### 4.2 Uncertainty decomposition results

As discussed in Section 2.3, CREDO provides a natural disentanglement of uncertainty components, yielding a layer of interpretability over other conformal methods. To validate this decomposition, we compare the proportion of

epistemic uncertainty—defined as the ratio of epistemic inflation to total non-conformalized interval width—between identified outliers and the 10% most central inliers across all 12 benchmarks.

We calculate the average normalized epistemic uncertainty per observation over 30 independent repetitions. The results, visualized via the boxplots in Figure 4 (Appendix B.5), demonstrate a consistent trend: outliers across diverse datasets tend to exhibit a higher proportion of epistemic uncertainty compared to inliers. This separation is particularly pronounced in six of the twelve datasets—four of which are small-data regimes with fewer than 10,000 samples—where data-scarce regions naturally harbor greater model ambiguity.

Table 1: **Efficiency of predictive sets as measured by SMIS (lower is better)**. SMIS summarizes the coverage–width trade-off by penalizing both interval length and misses outside the interval. Parentheses show  $2\times$  the standard deviation. Bold marks the best method within a 95% confidence interval (ties allowed). The sample size  $n$  of each dataset is shown next to its name. CREDO is consistently competitive on SMIS and the adaptive variant (with  $\gamma(x)$ ) is often best, suggesting improved efficiency without sacrificing calibration.

Dataset (n)	CREDO	CREDO (adap.)	CQR	CQR-r	UACQRS	UACQRP	EPIC
concrete (1030)	<b>27.59 (0.75)</b>	<b>26.49 (0.73)</b>	28.56 (0.92)	35.49 (1.55)	36.52 (1.42)	40.94 (2.06)	<b>27.51 (0.82)</b>
airfoil (1503)	11.37 (0.35)	11.25 (0.30)	10.51 (0.26)	13.68 (0.69)	12.68 (0.46)	14.74 (0.72)	<b>9.95 (0.24)</b>
winewhite (1599)	3.01 (0.03)	<b>2.88 (0.03)</b>	2.96 (0.03)	2.99 (0.03)	<b>2.92 (0.03)</b>	3.01 (0.03)	<b>2.89 (0.03)</b>
star $\times 10^2$ (2161)	9.92 (0.14)	<b>9.75 (0.11)</b>	10.08 (0.17)	11.33 (0.30)	<b>9.56 (0.14)</b>	<b>9.68 (0.17)</b>	10.06 (0.17)
winered (4898)	<b>2.74 (0.05)</b>	<b>2.66 (0.05)</b>	2.98 (0.07)	3.14 (0.09)	<b>2.77 (0.06)</b>	2.82 (0.06)	2.82 (0.06)
cycle (9568)	18.27 (0.19)	17.65 (0.14)	15.30 (0.16)	15.39 (0.17)	15.63 (0.16)	16.30 (0.22)	<b>15.29 (0.17)</b>
electric $\times 10^{-2}$ (10000)	<b>3.69 (0.16)</b>	<b>3.52 (0.14)</b>	4.41 (0.10)	4.71 (0.11)	5.44 (0.18)	6.01 (0.24)	4.30 (0.09)
meps19 (15781)	61.77 (1.40)	<b>57.21 (1.50)</b>	<b>58.82 (2.09)</b>	<b>58.59 (2.07)</b>	<b>56.45 (1.85)</b>	<b>58.82 (2.04)</b>	<b>57.91 (2.04)</b>
superconductivity (21263)	49.76 (0.54)	<b>44.17 (0.51)</b>	<b>43.76 (0.35)</b>	<b>43.79 (0.34)</b>	45.26 (0.39)	47.57 (0.36)	<b>43.67 (0.34)</b>
homes $\times 10^4$ (21613)	46.19 (0.46)	43.21 (0.37)	42.81 (0.51)	<b>42.60 (0.48)</b>	43.25 (0.50)	44.33 (0.57)	<b>41.72 (0.47)</b>
protein (45730)	15.22 (0.05)	<b>14.74 (0.06)</b>	15.17 (0.05)	15.17 (0.05)	15.33 (0.05)	15.77 (0.05)	15.12 (0.05)
WEC $\times 10^4$ (54000)	9.67 (0.08)	<b>8.67 (0.07)</b>	12.67 (0.12)	12.67 (0.12)	12.67 (0.12)	13.53 (0.12)	12.24 (0.11)

Table 2: **Adaptivity to outliers via the interval-length ratio (ILR; higher is better)**. ILR is the ratio of the average prediction-interval length on test-set outliers to the average length on test-set inliers. Parentheses show  $2\times$  the standard deviation. Bold marks the best method within a 95% confidence interval (ties allowed). The sample size  $n$  of each dataset is shown next to its name. CREDO typically achieves higher ILR, with the largest gains on small- $n$  datasets where epistemic uncertainty is most pronounced, indicating more targeted widening when data are scarce.

Dataset (n)	CREDO	CREDO (adap.)	CQR	CQR-r	UACQRS	UACQRP	EPIC
concrete (1030)	<b>1.09 (0.07)</b>	<b>1.15 (0.07)</b>	0.83 (0.05)	0.73 (0.07)	0.95 (0.02)	1.00 (0.03)	0.92 (0.05)
airfoil (1503)	<b>1.23 (0.10)</b>	<b>1.21 (0.10)</b>	1.06 (0.07)	<b>1.09 (0.11)</b>	1.05 (0.04)	1.07 (0.04)	<b>1.10 (0.07)</b>
winewhite (1599)	<b>1.11 (0.03)</b>	<b>1.11 (0.03)</b>	0.96 (0.02)	0.95 (0.02)	1.03 (0.02)	1.04 (0.01)	1.02 (0.03)
star (2161)	<b>0.99 (0.02)</b>	<b>0.99 (0.01)</b>	0.90 (0.02)	0.86 (0.03)	<b>1.00 (0.01)</b>	<b>1.00 (0.01)</b>	0.91 (0.02)
winered (4898)	<b>1.24 (0.06)</b>	<b>1.25 (0.06)</b>	0.88 (0.03)	0.83 (0.04)	1.01 (0.02)	1.01 (0.02)	1.02 (0.05)
cycle (9568)	1.00 (0.02)	<b>1.05 (0.02)</b>	0.88 (0.02)	0.87 (0.02)	0.89 (0.02)	0.95 (0.02)	0.89 (0.02)
electric (10000)	0.96 (0.02)	0.96 (0.02)	<b>1.00 (0.02)</b>	<b>1.00 (0.03)</b>	<b>1.01 (0.01)</b>	<b>1.02 (0.01)</b>	<b>1.00 (0.03)</b>
meps19 (15781)	<b>1.12 (0.07)</b>	<b>1.11 (0.08)</b>	<b>1.13 (0.06)</b>	<b>1.14 (0.06)</b>	<b>1.13 (0.05)</b>	<b>1.11 (0.05)</b>	<b>1.13 (0.06)</b>
superconductivity (21263)	<b>1.10 (0.03)</b>	1.09 (0.03)	<b>1.14 (0.03)</b>	<b>1.15 (0.03)</b>	<b>1.12 (0.03)</b>	<b>1.14 (0.03)</b>	<b>1.15 (0.03)</b>
homes (21613)	<b>1.64 (0.08)</b>	<b>1.64 (0.08)</b>	<b>1.36 (0.04)</b>	<b>1.40 (0.05)</b>	<b>1.36 (0.04)</b>	<b>1.44 (0.05)</b>	<b>1.50 (0.06)</b>
protein (45730)	<b>1.02 (0.01)</b>	<b>1.03 (0.01)</b>	0.99 (0.01)	0.99 (0.01)	0.99 (0.01)	1.00 (0.01)	1.00 (0.01)
WEC (54000)	<b>1.25 (0.03)</b>	<b>1.25 (0.03)</b>	1.16 (0.02)	1.16 (0.02)	1.16 (0.02)	1.16 (0.02)	1.21 (0.02)

These findings directly complement the ILR results from the previous section, providing a mechanistic explanation for why CREDO produces wider intervals for atypical points. By confirming that the credal envelope selectively expands in regions of low covariate support, these results indicate that our decomposition successfully isolates local epistemic uncertainty from global aleatoric noise.

## 5 Final Remarks

We introduced CREDO, a regression conformal predictor that makes *local epistemic uncertainty* explicit through covariate-dependent credal envelopes, while retaining split conformal’s finite-sample, distribution-free marginal coverage. By separating roles—credal modeling for epistemic structure and conformal calibration for validity—the resulting intervals are interpretable and admit a practical decomposition into aleatoric, epistemic, and calibration components, making it easier to diagnose *why* uncertainty is large at a given  $x$ .

The connections made in this paper open several avenues. On the modeling side,  $\mathcal{F}_0(x)$  could be built from predictive distributions induced by multiple priors or hyperpriors, alternative likelihood families, or ensembles, thereby representing model ambiguity beyond standard parameter uncertainty. For instance, in a Gaussian process, one could define a local credal set by taking the union of posterior predictive distributions obtained under different kernels and bandwidths. On the set-construction side, one can replace central-quantile envelopes with HPD/IHDR-style regions or other credal summaries better suited to skewed or multimodal conditionals, and then conformalize via an appropriate distance-to-region score. From a scalability perspective, deep kernel learning and learned embeddings  $\phi$  offer a path to faster and more faithful data-support measures for  $\gamma(x)$ . Finally, the same credal-conformal recipe should extend naturally to classification and structured outputs, where epistemic effects are often even more pronounced, and to decision-focused variants that tune the credal or conformal components for downstream utility subject to coverage constraints. Code implementing CREDO and reproducing the experiments is available at <https://github.com/Monoxido45/CREDO>

## Acknowledgements

S. J. S. was supported by the UKRI Turing AI World-Leading Researcher Fellowship, [EP/W002973/1]. R. I. is grateful for the financial support of CNPq (422705/2021-7, 305065/2023-8 and 403458/2025-0) and FAPESP (grant 2023/07068-1). L. M. C. C. is grateful for the financial support of FAPESP (grants 2022/08579-7 and 2025/06168-8). F. W. was supported by the Engineering and Physical Sciences Research Council [EP/Y030826/1]. B. M. R. is grateful for the financial support of FAPESP (grant 2025/04853-5).

## References

- Joaquin Abellan, George Jiri Klir, and Serafin Moral. Disaggregated total uncertainty measure for credal sets. *International Journal of General Systems*, 1(35):29–44, 2006.
- Anastasios N. Angelopoulos and Stephen Bates. A gentle introduction to conformal prediction and distribution-free uncertainty quantification. arXiv preprint arXiv:2107.07511, 2021.
- Thomas Augustin, Frank PA Coolen, Gert De Cooman, and Matthias CM Troffaes. *Introduction to imprecise probabilities*, volume 591. John Wiley & Sons, 2014.
- Nicola Barileto, Nhat Ho, and Alessandro Rinaldo. Conformalized bayesian inference, with applications to random partition models. *arXiv preprint arXiv:2511.05746v1*, 2025. URL <https://arxiv.org/abs/2511.05746v1>.
- Jose M Bernardo and Adrian FM Smith. *Bayesian theory*, volume 405. John Wiley & Sons, 2009.
- Markus M Breunig, Hans-Peter Kriegel, Raymond T Ng, and Jörg Sander. Lof: identifying density-based local outliers. In *Proceedings of the 2000 ACM SIGMOD international conference on Management of data*, pages 93–104, 2000.
- Luben Cabezas, Vagner S Santos, Thiago R Ramos, Pedro LC Rodrigues, and Rafael Izbicki. Cp4sbi: Local conformal calibration of credible sets in simulation-based inference. *arXiv preprint arXiv:2508.17077*, 2025a.
- Luben M. C. Cabezas, Mateus P. Otto, Rafael Izbicki, and Rafael B. Stern. Regression trees for fast and adaptive prediction intervals. *Information Sciences*, 686:121369, 2025b.
- Luben M. C. Cabezas, Vagner S. Santos, Thiago R. Ramos, and Rafael Izbicki. Epistemic uncertainty in conformal scores: A unified approach, 2025c. Manuscript (UAI submission).
- Michele Caprio. The joys of categorical conformal prediction, 2025. URL <https://arxiv.org/abs/2507.04441>.
- Michele Caprio and Teddy Seidenfeld. Constriction for sets of probabilities. In *International Symposium on Imprecise Probability: Theories and Applications*, pages 84–95. PMLR, 2023.
- Michele Caprio, Yusuf Sale, and Eyke Hüllermeier. Conformal prediction regions are imprecise highest density regions, 2025a. URL <https://arxiv.org/abs/2502.06331>.
- Michele Caprio, David Stutz, Shuo Li, and Arnaud Doucet. Conformalized credal regions for classification with ambiguous ground truth, 2025b. URL <https://arxiv.org/abs/2411.04852>.
- Leonardo Cella and Ryan Martin. Validity, consonant plausibility measures, and conformal prediction. *International Journal of Approximate Reasoning*, 141:110–130, February 2022. ISSN 0888-613X. doi: 10.1016/j.ijar.2021.07.013. URL <http://dx.doi.org/10.1016/j.ijar.2021.07.013>.
- Siu Lun Chau, Soroush H. Zargarbashi, Yusuf Sale, and Michele Caprio. Quantifying epistemic predictive uncertainty in conformal prediction, 2026. URL <https://arxiv.org/abs/2602.01667>.
- Hugh A. Chipman, Edward I. George, and Robert E. McCulloch. Bart: Bayesian additive regression trees. *The Annals of Applied Statistics*, 4(1):266–298, 2010. doi: 10.1214/09-AOAS285.
- Mathieu Cochetoux, Julien Moreau, and Franck Davoine. Uncertainty-aware online extrinsic calibration: A conformal prediction approach, 2025. arXiv:2501.06878.
- Anna Veronika Dorogush, Vasily Ershov, and Andrey Gulin. Catboost: gradient boosting with categorical features support. *arXiv preprint arXiv:1810.11363*, 2018.
- Edwin Fong and Chris C. Holmes. Conformal bayesian computation. In *Advances in Neural Information Processing Systems*, volume 34, pages 18268–18279, 2021.
- Yarin Gal and Zoubin Ghahramani. Dropout as a bayesian approximation: Representing model uncertainty in deep learning. In *International Conference on Machine Learning*, Proceedings of Machine Learning Research, pages 1050–1059. PMLR, 2016.
- Tilmann Gneiting and Adrian E Raftery. Strictly proper scoring rules, prediction, and estimation. *Journal of the American statistical Association*, 102(477):359–378, 2007.

- Eyke Hüllermeier and Willem Waegeman. Aleatoric and epistemic uncertainty in machine learning: An introduction to concepts and methods. *Machine Learning*, 110:457–506, 2021.
- Rafael Izbicki. *Machine Learning Beyond Point Predictions: Uncertainty Quantification*. 1st edition, 2025. ISBN 978-65-01-20272-3.
- Rafael Izbicki, Gilson Shimizu, and Rafael Stern. Flexible distribution-free conditional predictive bands using density estimators. In *International Conference on Artificial Intelligence and Statistics*, pages 3068–3077. PMLR, 2020.
- Rafael Izbicki, Gilson Shimizu, and Rafael B. Stern. Cd-split and hpd-split: Efficient conformal regions in high dimensions. *Journal of Machine Learning Research*, 23(87):1–32, 2022.
- Edgar Jaber, Vincent Blot, Nicolas Brunel, Vincent Chabridon, Emmanuel Remy, Bertrand Iooss, Didier Lucor, Mathilde Mougeot, and Alessandro Leite. Conformal approach to gaussian process surrogate evaluation with coverage guarantees, 2024. arXiv:2401.07733.
- Laurens Jansen. Robust bayesian inference under model misspecification. Master’s thesis, Leiden University, 2013. Chapter 4.5.
- Alireza Javanmardi, David Stutz, and Eyke Hüllermeier. Conformalized credal set predictors. In A. Globerson, L. Mackey, D. Belgrave, A. Fan, U. Paquet, J. Tomczak, and C. Zhang, editors, *Advances in Neural Information Processing Systems*, volume 37, pages 116987–117014. Curran Associates, Inc., 2024. doi: 10.52202/079017-3714. URL [https://proceedings.neurips.cc/paper\\_files/paper/2024/file/d42a8bf2f40555d4a5120300f98c88f6-Paper-Conference.pdf](https://proceedings.neurips.cc/paper_files/paper/2024/file/d42a8bf2f40555d4a5120300f98c88f6-Paper-Conference.pdf).
- Jing Lei, Max G’Sell, Alessandro Rinaldo, Ryan J. Tibshirani, and Larry Wasserman. Distribution-free predictive inference for regression. *Journal of the American Statistical Association*, 113(523):1094–1111, 2018.
- Isaac Levi. *The Enterprise of Knowledge*. London, UK : MIT Press, 1980.
- Yaniv Ovadia, Emily Fertig, Jie Ren, Zachary Nado, D Sculley, Sebastian Nowozin, Joshua V. Dillon, Balaji Lakshminarayanan, and Jasper Snoek. Can you trust your model’s uncertainty? evaluating predictive uncertainty under dataset shift, 2019. URL <https://arxiv.org/abs/1906.02530>.
- Harris Papadopoulos, Kostas Proedrou, Volodya Vovk, and Alex Gammerman. Inductive confidence machines for regression. In *Machine Learning: ECML 2002*, pages 345–356. Springer, 2002.
- Aurélien Pion and Emmanuel Vazquez. Gaussian process interpolation with conformal prediction: Methods and comparative analysis. In *LOD 2024: International Conference on Machine Learning, Optimization, and Data Science*, 2024.
- Yaniv Romano, Evan Patterson, and Emmanuel J. Candès. Conformalized quantile regression. *Advances in Neural Information Processing Systems*, 2019.
- Raphael Rossellini, Rina Foygel Barber, and Rebecca Willett. Integrating uncertainty awareness into conformalized quantile regression. In *International Conference on Artificial Intelligence and Statistics*, pages 1540–1548. PMLR, 2024.
- Teddy Seidenfeld and Larry Wasserman. Dilation for Sets of Probabilities. *The Annals of Statistics*, 21(3):1139 – 1154, 1993. doi: 10.1214/aos/1176349254. URL <https://doi.org/10.1214/aos/1176349254>.
- Matteo Sesia and Emmanuel J Candès. A comparison of some conformal quantile regression methods. *Stat*, 9(1): e261, 2020.
- Glenn Shafer and Vladimir Vovk. A tutorial on conformal prediction. *Journal of Machine Learning Research*, 9: 371–421, 2008.
- Matthias C. M. Troffaes and Gert de Cooman. *Lower Previsions*. Wiley Series in Probability and Statistics. John Wiley & Sons, Chichester, United Kingdom, 2014. ISBN 978-0-470-72377-7. doi: 10.1002/9781118762622. URL <https://doi.org/10.1002/9781118762622>.
- Laurens Van der Maaten and Geoffrey Hinton. Visualizing data using t-sne. *Journal of machine learning research*, 9(11), 2008.

- Vladimir Vovk, Alex Gammerman, and Glenn Shafer. *Algorithmic Learning in a Random World*. Springer, 2005.
- Vladimir Vovk, Alexander Gammerman, and Glenn Shafer. *Algorithmic Learning in a Random World*. Springer Nature, 2nd edition, 2022.
- Peter Walley. *Statistical Reasoning with Imprecise Probabilities*. Chapman and Hall/CRC, 1991.
- Meijiang Wang, Jingyu He, and P. Richard Hahn. Local gaussian process extrapolation for bart models with applications to causal inference. arXiv preprint arXiv:2204.10963, 2022. Version 2 (revised Feb 24, 2023).
- Andrew Gordon Wilson, Zhiting Hu, Ruslan Salakhutdinov, and Eric P Xing. Deep kernel learning. In *Artificial intelligence and statistics*, pages 370–378. PMLR, 2016.
- Fanyi Wu, Veronika Lohmanova, Samuel Kaski, and Michele Caprio. Bayesian conformal prediction as a decision risk problem, 2026. URL <https://arxiv.org/abs/2602.03331>.
- Puning Zhao and Lifeng Lai. Analysis of knn density estimation. *IEEE Transactions on Information Theory*, 68(12):7971–7995, 2022.

# Appendix

## A CREDO algorithms

This section presents the algorithmic framework for CREDO. Algorithm 1 details the construction and conformalization of the credal envelope, while Algorithm 2 specifies the adaptive  $\gamma(x)$  scheme. Finally, Algorithm 3 outlines the decomposition of the prediction intervals into aleatoric and epistemic components.

---

**Algorithm 1** CREDO: Conformalized credal regression intervals via endpoint-trimmed posterior envelopes

---

**Require:** Exchangeable data  $D = \{(X_i, Y_i)\}_{i=1}^n$ ; split sizes with  $|D_{\text{cal}}| = m$ ; query observation  $x$ .  
**Require:** Levels  $\alpha_0 \in (0, 1)$  (credal nominal) and  $\alpha \in (0, 1)$  (conformal).  
**Require:** Conditional model  $\{F_\theta(\cdot | x) : \theta \in \Theta\}$ , prior  $\pi(\theta)$ , posterior sampler; MC size  $B$ .  
**Require:** Trimming: either constant  $\gamma \in (0, 1)$  or covariate-dependent  $\gamma(x)$  using Algorithm 2.  
**Ensure:** For any query covariate  $x$ , output  $C(x) = [\ell(x) - \hat{\tau}, u(x) + \hat{\tau}]$  and (optionally) the uncertainty decomposition.

- 1: **Split:** Randomly split  $D$  into  $D_{\text{tr}}$  and  $D_{\text{cal}}$  (size  $m$ ).
- 2: **Posterior:** Fit on  $D_{\text{tr}}$  to obtain  $\pi(\theta | D_{\text{tr}})$ ; draw  $\theta^{(1)}, \dots, \theta^{(B)} \sim \pi(\theta | D_{\text{tr}})$ .
- 3: **function** ENVELOPE( $x$ )
- 4:   **for**  $b = 1$  to  $B$  **do**
- 5:      $q_L^{(b)}(x) \leftarrow F_{\theta^{(b)}}^{-1}(\alpha_0/2 | x)$ ;    $q_U^{(b)}(x) \leftarrow F_{\theta^{(b)}}^{-1}(1 - \alpha_0/2 | x)$ .
- 6:   **end for**
- 7:   **if** Constant  $\gamma$  **then**
- 8:      $\gamma(x) \leftarrow \gamma$
- 9:   **end if**
- 10:    $C_L(x) \leftarrow \text{Quantile}_{\gamma(x)/2}(\{q_L^{(b)}(x)\}_{b=1}^B)$ ;  $C_U(x) \leftarrow \text{Quantile}_{1-\gamma(x)/2}(\{q_U^{(b)}(x)\}_{b=1}^B)$ .
- 11:    $\ell(x) \leftarrow C_L(x)$ ;  $u(x) \leftarrow C_U(x)$  ▷ trimmed endpoint envelope (3)
- 12:   **return**  $(\ell(x), u(x), \{q_L^{(b)}(x), q_U^{(b)}(x)\}_{b=1}^B)$ .
- 13: **end function**
- 14: **Conformal calibration on**  $D_{\text{cal}}$ :
- 15: **for all**  $(x_i, y_i) \in D_{\text{cal}}$  **do**
- 16:    $(\ell_i, u_i, -) \leftarrow \text{ENVELOPE}(x_i)$ .
- 17:    $s_i \leftarrow \max\{\ell_i - y_i, y_i - u_i\}$  ▷ distance-to-envelope score (2)
- 18: **end for**
- 19:  $\hat{\tau} \leftarrow$  the  $\lceil (m+1)(1-\alpha) \rceil$ -th order statistic of  $\{s_i\}_{i=1}^m$ .
- 20: **Prediction for a new covariate**  $x$ :
- 21:  $(\ell(x), u(x), \{q_L^{(b)}(x), q_U^{(b)}(x)\}) \leftarrow \text{ENVELOPE}(x)$ .
- 22: **if** requires uncertainty decomposition at  $x$  **then**
- 23:   Run Algorithm 3 with input  $((\ell(x), u(x)), \{q_L^{(b)}(x), q_U^{(b)}(x)\}_{b=1}^B)$
- 24:   Returns  $\hat{U}_A(x), \hat{U}_E(x)$
- 25: **end if**
- 26: **Output**  $C(x) = [\ell(x) - \hat{\tau}, u(x) + \hat{\tau}]$  and  $\hat{U}_A(x), \hat{U}_E(x)$  if demanded ▷ final set (2)

---

---

**Algorithm 2** Adaptive  $\gamma$ 

---

**Require:** Training set  $D_{tr}$  and observation  $x$ .

**Require:** Representation  $\phi(\cdot)$ ,  $k$ , constants  $\gamma_{\min}, \gamma_{\max}, \tau_\gamma, m_\gamma$ , and  $\varepsilon > 0$ .

**Ensure:** For any query covariate  $x$ , output  $\gamma(x)$ .

- 1: For each training covariate  $X_i$  in  $D_{tr}$ , compute  $r_k(X_i) := \|\phi(X_i) - \phi(X_{(k)}(X_i))\|$ .
  - 2: Set reference quantiles  $q_{lo} = \text{Quantile}_{0.50}(\{r_k(X_i)\})$  and  $q_{hi} = \text{Quantile}_{0.95}(\{r_k(X_i)\})$ .
  - 3: Find  $X_{(k)}(x)$  as the  $k$ -th nearest neighbor of  $x$  among  $\{X_i : (X_i, Y_i) \in D_{tr}\}$ .
  - 4:  $r_k(x) \leftarrow \|\phi(x) - \phi(X_{(k)}(x))\|$ .
  - 5:  $sc(x) \leftarrow \frac{r_k(x) - q_{lo}}{q_{hi} - q_{lo} + \varepsilon}$ . ▷ Defining scarcity score
  - 6: **Output**  $\gamma(x) \leftarrow \gamma_{\max} - (\gamma_{\max} - \gamma_{\min}) \sigma\left(\frac{sc(x) - m_\gamma}{\tau_\gamma}\right)$ . ▷ Use scarcity score to compute  $\gamma$
- 

---

**Algorithm 3** Uncertainty Decomposition

---

**Require:** Lower and upper envelope bounds at observation  $x$ ,  $(\ell(x), u(x))$ .

**Require:** Lower and upper quantile vectors at observation  $x$ ,  $\{q_L^{(b)}(x), q_U^{(b)}(x)\}_{b=1}^B$ .

**Ensure:** For any query covariate  $x$ , output  $(\hat{U}_A(x), \hat{U}_E(x))$ .

- 1: **Optional uncertainty decomposition at  $x$ :**
  - 2:  $\hat{U}_A(x) \leftarrow \frac{1}{B} \sum_{b=1}^B (q_U^{(b)}(x) - q_L^{(b)}(x))$ .
  - 3:  $\hat{U}_E(x) \leftarrow (u(x) - \ell(x)) - \hat{U}_A(x)$ ; conformal term =  $2\hat{\tau}$ .
  - 4: (So  $|C(x)| = \hat{U}_A(x) + \hat{U}_E(x) + 2\hat{\tau}$ ).
  - 5: **Output**  $\hat{U}_A(x), \hat{U}_E(x)$ .
- 

## B Additional results and experiments details

In this section, we provide a comprehensive overview of our evaluation metrics, baseline architectures, and extended comparative results. We also detail the outlier detection methodology employed and present uncertainty decomposition analyses for both simulated and real-world datasets. Table 3 summarizes the regression benchmarks used throughout our study; these datasets are standard in the conformal prediction literature [Romano et al., 2019, Rossellini et al., 2024] and offer a diverse range of sample sizes and dimensionalities. Together, they provide a robust testbed for evaluating the performance, adaptivity, and interpretability of the proposed approach.

Table 3: Benchmark Datasets Overview. We summarize the sample size ( $n$ ), feature count ( $p$ ), and the original scientific domain of each benchmark.

Dataset	$n$	$p$	Scientific Domain	Data Source
Concrete	1,030	8	Civil Engineering	UCI Repository
Airfoil	1,503	5	Aeroacoustics	UCI Repository
Wine White	1,599	11	Enology	UCI Repository
Star	2,161	48	Pedagogy	Harvard Dataverse
Wine Red	4,898	11	Enology	UCI Repository
Cycle	9,568	4	Thermodynamics	UCI Repository
Electric	10,000	12	Power Systems	UCI Repository
Meps19	15,781	141	Health Economics	AHRQ (MEPS)
Superconductivity	21,263	81	Condensed Matter Physics	UCI Repository
Homes	21,613	17	Econometrics	Kaggle
Protein	45,730	8	Structural Bioinformatics	UCI Repository
Wave Energy (WEC)	54,000	49	Renewable Energy	UCI Repository

## B.1 Outlier detection method

To assess how prediction sets adapt to data scarcity, we categorize test set observations using a model-agnostic density approach. We first project the feature space into two dimensions using t-SNE [Van der Maaten and Hinton, 2008] and then apply the Local Outlier Factor (LOF) method [Breunig et al., 2000]. Using  $k = 15$  nearest neighbors and a 5% contamination rate, we identify a set of local anomalies to serve as our outlier group.

For a robust comparative analysis, we contrast these outliers against two specific inlier reference groups:

- **Interval Ratio (ILR):** We compare outliers against the 20% most central inliers (those with the lowest LOF scores) to assess global adaptivity across all benchmarks.
- **Uncertainty Decomposition:** We narrow the focus to the 10% most central inliers to provide a more rigorous baseline for validating the disentanglement of epistemic and aleatoric signals.

The LOF score provides a structured, model-agnostic characterization of data density, serving as an external proxy for covariate support. It is important to distinguish this evaluation procedure from the adaptive  $\gamma(x)$  mechanism within CREDO. While  $\gamma(x)$  is an intrinsic component used to manage model ambiguity during inference, LOF is employed here strictly as an independent diagnostic tool for categorization in the test set. This ensures that our assessment of epistemic uncertainty—specifically the expectation that outliers in sparse regions yield wider sets while inliers in dense regions yield narrower ones—is verified against a standard external baseline, rather than being an artifact of the model’s internal representations.

## B.2 Evaluation metrics details

Let  $\hat{C}(\mathbf{X})$  denote a generic prediction set. Given a test set  $\{(\mathbf{X}_i, Y_i)\}_{i=1}^m$ , we evaluate the performance of all methods using three primary categories of metrics: reliability, efficiency, and epistemic awareness.

**1. Reliability and Coverage Accuracy** To verify that the nominal coverage  $1 - \alpha$  is maintained both globally and in data-sparse regions, we report:

- **Average Marginal Coverage (AMC):** The empirical proportion of test points covered by the prediction sets:

$$\text{AMC} = \frac{1}{m} \sum_{i=1}^m \mathbb{I}(Y_i \in \hat{C}(\mathbf{X}_i)).$$

- **Average Coverage on Outliers (ACO):** The empirical coverage calculated exclusively over the set of detected outliers  $I_{\text{out}}$  (see Section B.1):

$$\text{ACO} = \frac{1}{|I_{\text{out}}|} \sum_{i \in I_{\text{out}}} \mathbb{I}(Y_i \in \hat{C}(\mathbf{X}_i)).$$

Maintaining ACO near the nominal level  $1 - \alpha$  indicates that the method remains reliable even under significant sparsity.

**2. Conditional Coverage Efficiency** To evaluate the quality of the intervals beyond marginal coverage, we employ proxies for conditional validity:

- **Scaled Mean Interval Score (SMIS):** Introduced by Gneiting and Raftery [2007], this score evaluates the trade-off between interval width and miscoverage:

$$\begin{aligned} \text{SMIS} = \frac{1}{m} \sum_{i=1}^m & \left[ \left( \max \hat{C}(\mathbf{X}_i) - \min \hat{C}(\mathbf{X}_i) \right) \right. \\ & + \frac{2}{\alpha} \cdot \left( \min \hat{C}(\mathbf{X}_i) - Y_i \right) \cdot \mathbb{I} \left\{ Y_i < \min \hat{C}(\mathbf{X}_i) \right\} \\ & \left. + \frac{2}{\alpha} \cdot \left( Y_i - \max \hat{C}(\mathbf{X}_i) \right) \cdot \mathbb{I} \left\{ Y_i > \max \hat{C}(\mathbf{X}_i) \right\} \right], \end{aligned}$$

where  $\min \hat{C}(\mathbf{X})$  and  $\max \hat{C}(\mathbf{X})$  are the interval endpoints. By penalizing both excessive width and miscoverage, SMIS identifies methods that achieve high efficiency per unit of coverage, which translates into more locally-adaptive methods. Since this proper scoring rule is minimized when the interval boundaries match the true conditional quantiles, it serves as a proxy for *conditional coverage* adaptivity.

### 3. Epistemic Awareness

- **Outlier-to-Inlier Length Ratio (ILR)** [Cabezas et al., 2025c]: This metric assesses how the method distinguishes between data-rich and data-sparse regions. Let  $\bar{W}(I) = \frac{1}{|I|} \sum_{i \in I} (\max \hat{C}(\mathbf{X}_i) - \min \hat{C}(\mathbf{X}_i))$  be the average width over an index set  $I$ . The ILR is defined as:

$$\text{ILR} = \frac{\bar{W}(I_{\text{out}})}{\bar{W}(I_{\text{in}})},$$

where  $I_{\text{out}}$  contains all detected outliers (5% contamination) and  $I_{\text{in}}$  contains the 20% most central inliers. A higher ILR indicates successful identification of epistemic uncertainty through selective interval widening in sparse regions.

## B.3 Baselines details

### Conformal Baselines and Architectures

We evaluate CREDO against a range of state-of-the-art conformal regressors. All methods utilize CatBoost [Dorogush et al., 2018] as the underlying quantile regression model. The baselines are categorized as follows:

- **CQR & CQR-r** [Romano et al., 2019, Sesia and Candès, 2020]: These represent the standard for conformal quantile regression. While CQR provides a global calibration of quantile estimates, CQR-r incorporates a randomized scaling factor to enhance local adaptivity. Both methods focus primarily on capturing aleatoric uncertainty through the base quantile regressor.
- **UACQR-S & UACQR-P** [Rossellini et al., 2024]: These variants integrate epistemic uncertainty by constructing an ensemble of  $B = 1000$  base models. **UACQR-S** (Standardized) inflates the conformal score using the ensemble standard deviation, effectively widening intervals in regions of high model disagreement. **UACQR-P** (Percentile) utilizes order statistics from the ensemble to derive a more conservative, disagreement-aware conformal set.
- **EPICScore (MDN)** [Cabezas et al., 2025c]: This method integrates epistemic uncertainty through score rectification, leveraging the predictive conditional distribution of the conformity scores. Instead of using the raw conformal scores, EPICScore defines a new transformed score based on the predictive posterior distribution of the original scores. We utilize the **Mixture Density Network (MDN)** variant, which models the score distribution as a mixture of Gaussians and employs MC-Dropout [Gal and Ghahramani, 2016] to capture model ambiguity and estimate the posterior predictive distribution.

### Implementation Details and Hyperparameters

The experimental configurations for the baselines are detailed below:

- **CatBoost Base Model:** Following standard practice and ensuring a robust model, we fix the tree depth to 6,  $L_2$  leaf regularization to 3, and the bagging temperature to 1. The models are trained for 1000 iterations with an auto-tuned learning rate.
- **EPICScore MDN:** For the EPICScore baseline, we implement a Mixture Density Network (MDN) trained specifically to model the distribution of the conformity scores generated by the CatBoost base model. The MDN architecture consists of two hidden layers with 64 nodes each and approximates the predictive distribution of these scores as a mixture of 5 Gaussian components. To ensure convergence while preventing overfitting, the MDN is trained for a maximum of 2000 epochs with an early stopping patience of 50 iterations. We utilize a learning rate of 0.001 and a dropout rate of 0.5 to facilitate MC-dropout-based epistemic estimation. The training employs an adaptive batch size: 40 for smaller samples, 130 for larger sets such as *Superconductivity*, and 250 for the *WEC* benchmark.
- **Ensemble Settings:** The UACQR variants utilize the same ensemble size of catboost,  $B = 1000$ , ensuring stable and robust estimation of the epistemic signals.

## B.4 Additional comparisons

The additional marginal coverage and coverage on test set outliers are respectively displayed on Tables 4 and 5. In general, all approaches respect the conformal marginal validity for every dataset in Table 4, while CREDO stands out in the outlier coverage, achieving the closest coverage in the majority of scenarios, confirming that the widening of intervals in outliers also corresponds to an improvement in coverage in these areas.

Table 4: **Marginal coverage on test data (target  $1 - \alpha$ ).** Entries report the mean empirical coverage over 30 runs; parentheses show  $2\times$  the standard deviation. All methods achieve coverage close to the nominal level, with small deviations due to finite-sample variability and random splitting.

Dataset (n)	CREDO	CREDO (adap.)	CQR	CQR-r	UACQRS	UACQRP	EPIC
concrete (1030)	0.91 (0.01)	0.90 (0.01)	0.90 (0.01)	0.89 (0.01)	0.90 (0.01)	0.90 (0.01)	0.90 (0.02)
airfoil (1503)	0.90 (0.01)	0.91 (0.01)	0.91 (0.01)	0.89 (0.01)	0.90 (0.01)	0.90 (0.01)	0.91 (0.01)
winewhite (1599)	0.90 (0.00)	0.90 (0.01)	0.91 (0.00)	0.90 (0.00)	0.90 (0.00)	0.90 (0.00)	0.90 (0.01)
star (2161)	0.90 (0.01)	0.90 (0.01)	0.90 (0.01)	0.90 (0.01)	0.90 (0.01)	0.90 (0.01)	0.91 (0.01)
winered (4898)	0.90 (0.01)	0.90 (0.01)	0.90 (0.01)	0.90 (0.01)	0.90 (0.01)	0.90 (0.01)	0.90 (0.01)
cycle (9568)	0.90 (0.00)	0.90 (0.00)	0.90 (0.00)	0.90 (0.00)	0.90 (0.00)	0.90 (0.00)	0.90 (0.01)
electric (10000)	0.90 (0.00)	0.90 (0.00)	0.90 (0.00)	0.90 (0.00)	0.90 (0.00)	0.90 (0.00)	0.90 (0.00)
meps19 (15781)	0.90 (0.00)	0.90 (0.00)	0.90 (0.00)	0.90 (0.00)	0.90 (0.00)	0.92 (0.01)	0.90 (0.00)
superconductivity (21263)	0.90 (0.00)	0.90 (0.00)	0.90 (0.00)	0.90 (0.00)	0.90 (0.00)	0.90 (0.00)	0.90 (0.00)
protein (45730)	0.90 (0.00)	0.90 (0.00)	0.90 (0.00)	0.90 (0.00)	0.90 (0.00)	0.90 (0.00)	0.90 (0.00)
homes (21613)	0.90 (0.00)	0.90 (0.00)	0.90 (0.00)	0.90 (0.00)	0.90 (0.00)	0.90 (0.00)	0.90 (0.00)
WEC (54000)	0.90 (0.00)	0.90 (0.00)	0.90 (0.00)	0.90 (0.00)	0.90 (0.00)	0.90 (0.00)	0.90 (0.00)

Table 5: **Coverage on test-set outliers (target  $1 - \alpha = 0.90$ ).** Outliers are defined using the criterion as in Appendix B.1. Entries report the mean outlier coverage over 30 runs; parentheses show  $2\times$  the standard deviation. Bold marks methods whose outlier coverage is closest to 0.90 within a 95% confidence interval. Both CREDO versions have the closest coverage to the nominal level in 9 out of 12 datasets, showcasing its adaptability to outlier regions and its adequacy to deal with epistemic uncertainty.

Dataset (n)	CREDO	CREDO (adap.)	CQR	CQR-r	UACQRS	UACQRP	EPIC
concrete (1030)	<b>0.92 (0.03)</b>	<b>0.92 (0.03)</b>	<b>0.87 (0.04)</b>	0.85 (0.05)	<b>0.88 (0.05)</b>	0.86 (0.04)	<b>0.87 (0.05)</b>
airfoil (1503)	<b>0.90 (0.04)</b>	<b>0.89 (0.03)</b>	<b>0.87 (0.04)</b>	<b>0.88 (0.05)</b>	<b>0.91 (0.04)</b>	<b>0.89 (0.04)</b>	<b>0.91 (0.03)</b>
winewhite (1599)	<b>0.90 (0.01)</b>	<b>0.89 (0.02)</b>	0.86 (0.02)	0.85 (0.02)	<b>0.89 (0.02)</b>	0.88 (0.01)	0.88 (0.02)
star (2161)	<b>0.88 (0.02)</b>	0.87 (0.02)	0.79 (0.04)	0.74 (0.04)	0.85 (0.03)	0.85 (0.02)	0.80 (0.03)
winered (4898)	<b>0.91 (0.03)</b>	<b>0.90 (0.03)</b>	0.82 (0.04)	0.80 (0.04)	0.84 (0.05)	0.84 (0.05)	0.83 (0.04)
cycle (9568)	<b>0.89 (0.02)</b>	<b>0.91 (0.01)</b>	0.85 (0.01)	0.84 (0.01)	0.86 (0.02)	0.88 (0.01)	0.86 (0.01)
electric (10000)	0.88 (0.01)	<b>0.89 (0.01)</b>	<b>0.91 (0.01)</b>	<b>0.90 (0.01)</b>	<b>0.90 (0.01)</b>	<b>0.90 (0.01)</b>	<b>0.91 (0.01)</b>
meps19 (15781)	<b>0.90 (0.01)</b>	<b>0.90 (0.01)</b>	<b>0.89 (0.01)</b>	<b>0.89 (0.01)</b>	<b>0.90 (0.01)</b>	0.92 (0.02)	<b>0.89 (0.01)</b>
superconductivity (21263)	0.92 (0.01)	<b>0.91 (0.01)</b>	0.87 (0.01)	0.89 (0.01)	0.87 (0.01)	0.88 (0.01)	0.88 (0.01)
homes (21613)	0.92 (0.01)	0.92 (0.01)	<b>0.89 (0.01)</b>	<b>0.90 (0.01)</b>	0.89 (0.01)	<b>0.90 (0.01)</b>	<b>0.90 (0.01)</b>
protein (45730)	<b>0.90 (0.01)</b>	<b>0.90 (0.01)</b>	0.89 (0.01)	0.89 (0.01)	0.89 (0.01)	0.89 (0.01)	0.89 (0.01)
WEC (54000)	<b>0.86 (0.01)</b>	0.84 (0.01)	0.85 (0.01)	0.85 (0.01)	0.85 (0.01)	0.85 (0.01)	0.84 (0.01)

## B.5 Uncertainty decomposition in real data

For the uncertainty decomposition experiments, we employ the adaptive CREDO version detailed in Section C.2 and categorize test observations using the density-based procedure described in Section B.1. We evaluate the effectiveness of this decomposition by comparing the percentage of epistemic uncertainty—averaged by observations across 30 experimental repetitions—between the identified outliers and the top 10% of inliers.

Figure 4 presents the resulting boxplots for all 12 regression benchmarks. We observe that outliers consistently exhibit higher normalized epistemic uncertainty than inliers in smaller datasets, such as *concrete*, *winewhite*, *winered*, and *cycle*. This trend aligns with the expectation that smaller sample sizes are more susceptible to regional sparsity, leading the credal envelope to correctly assign higher model ambiguity to isolated points. Conversely, in several high-dimensional or larger datasets like *homes*, *proteins*, and *WEC*, the differences between groups remain notable, albeit sometimes more subtle. This suggests that even with larger global sample sizes, the increased dimensionality preserves local regions of scarcity where epistemic uncertainty remains a dominant factor.

In instances where the disparity between inliers and outliers is negligible, the result can often be attributed to model specification constraints that induce uniform epistemic behavior regardless of local data density. Such cases

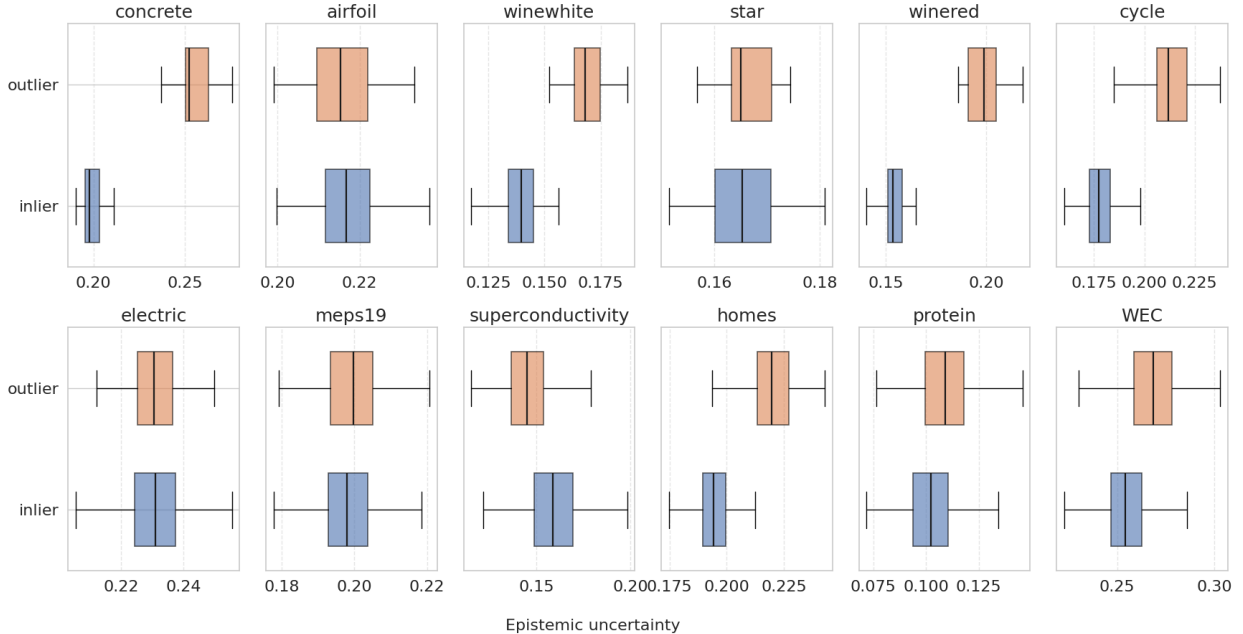


Figure 4: Percentage of Epistemic Uncertainty for outliers and inliers across real-world datasets using the QNN-based implementation of CREDO. The uncertainty decomposition successfully attributes a higher proportion of epistemic uncertainty to outliers compared to inliers, a distinction that is particularly pronounced in small-data domains (top row).

provide a valuable diagnostic for the base model’s representational limits: if the underlying architecture cannot distinguish between high-support and low-support regions, the credal envelope reflects this lack of discriminative power. Ultimately, these results validate the ability of CREDO to treat epistemic uncertainty as a spatially-aware signal, effectively identifying when prediction intervals are widened due to a genuine lack of information rather than inherent statistical noise.

## B.6 Simulated scenarios and Uncertainty decompositions

The simulated scenarios used in this work are specifically engineered to highlight the behavior of the credal envelope in regions of high data scarcity while simultaneously testing its stability in densely populated, heteroscedastic regions. We detail below the data-generating processes for the three scenarios used to evaluate the interpretability of CREDO:

- **Scenario 1** (Epistemic Gap): Features a piecewise non-linear mean function where the left and right domains are well-sampled, but the middle region ( $x \in [-0.2, 0.2]$ ) contains very few points (1% of the samples). The noise is kept constant and small ( $\sigma = 0.1$ ) to ensure that any interval widening in the gap is strictly attributed to epistemic uncertainty.
- **Scenario 2** (Heteroscedastic Scarcity): Defines a scarce region in the interval  $[0, 0.4]$  containing only 2% of the total samples. The noise profile is defined by a complex heteroscedastic function  $\sigma(x)$  that oscillates across four distinct regions: low variance ( $\sigma = 0.1$ ) for  $x \leq -0.3$ , moderate oscillating variance ( $\sigma(x) = 0.2 + 0.15|\sin(10x)|$ ) for  $x \in (-0.3, 0)$ , high oscillating variance ( $\sigma(x) = 0.7 + 0.3|\sin(12x)|$ ) in the scarce region, and back to moderate levels for  $x > 0.4$ .
- **Scenario 3** (Mixture Gaps): Uses a mixture of Gaussian clusters and uniform bands to create several disjoint dense and sparse regions: a dense left cluster ( $\mu = -1.8, \sigma = 0.35$ ), a dense right cluster ( $\mu = 1.6, \sigma = 0.45$ ), a sparse middle band ( $x \in [-0.4, 0.4]$ ), and extreme tail points for extrapolation pressure. The noise is sampled from a conditional mixture where a "shock" component (shifted, high-variance) occurs with a

probability  $p_{shock}(x)$  that increases significantly in the far tails and right regions, governed by a logistic sigmoid  $p_{shock}(x) = 0.05 + 0.35/(1 + e^{-(x-1.3)}) + 0.15 \cdot \mathbb{I}(|x| > 3.2)$ .

In the main text, Scenario 1 is utilized in Figure 1 to evaluate the capture of epistemic uncertainty and contrast the geometric behavior of CREDO against standard CQR. Scenario 2 is featured in Figure 3 to demonstrate the efficiency of the adaptive  $\gamma(x)$  scheme, showcasing its ability to produce more informative intervals in well-supported regions compared to a fixed hyperparameter.

To further validate the interpretability of our framework, we provide additional displays of the uncertainty decomposition for Scenarios 2 and 3 in Figure 5. These results demonstrate that CREDO successfully isolates the aleatoric core—even when that core is highly heteroscedastic or multi-modal—from the epistemic inflation triggered by the scarcity score. This confirms that the framework can distinguish between "risk" (known aleatoric noise) and "ambiguity" (lack of local information) in a consistent way.

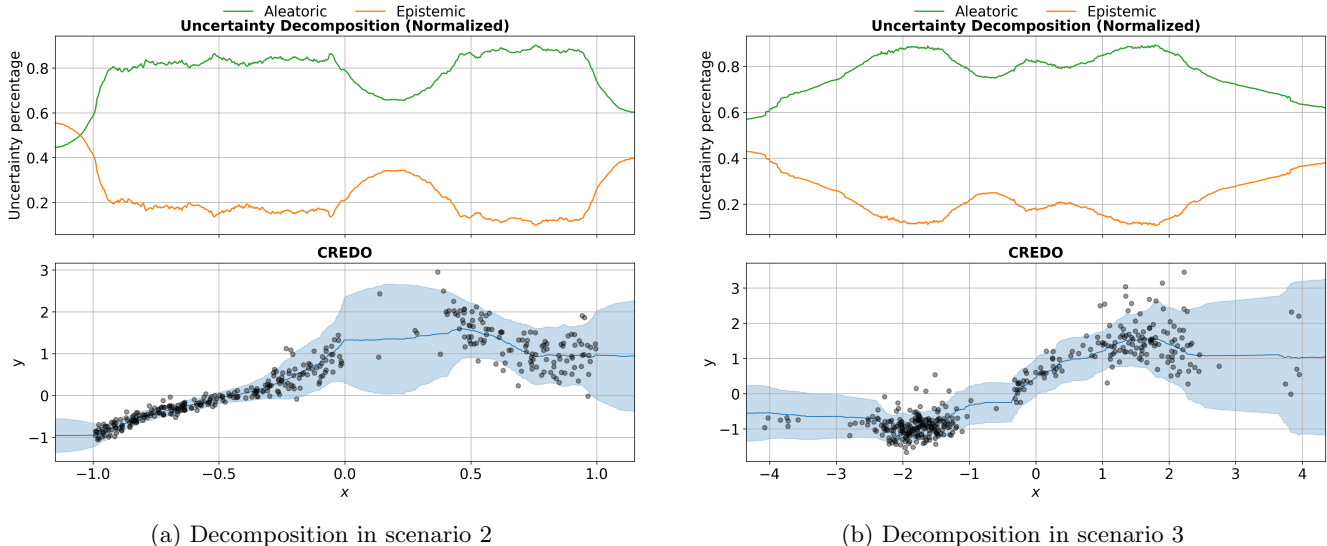


Figure 5: Normalized Uncertainty Decomposition for Scenarios 2 and 3. This figure illustrates the ability of CREDO to disentangle aleatoric and epistemic components under complex data-generating processes. In Scenario 2 (left), the decomposition successfully isolates the high epistemic inflation in the scarce region ( $x \in [0, 0.4]$ ) from the underlying oscillating heteroscedastic noise. Similarly, in Scenario 3 (right), the epistemic percentage peaks in the gaps between clusters and in the extrapolative tails, despite the presence of multi-modal "shock" noise components.

## C CREDO computational details

In this section, we give details on the architecture and the approach to derive the credal envelopes by using a Quantile Neural Network with dropout, as well as the standard parameter choices and heuristics for the adaptive gamma scheme. We also shed light on an alternative approach to building the credal envelopes by using BART, which was employed in some illustrations and toy examples of this work.

### C.1 QNN architecture and envelope

For the deep learning-based implementation of the credal envelope, we utilize a Quantile Neural Network (QNN) designed to produce the initial quantile estimates while capturing model uncertainty via dropout.

- **Network Architecture:** The model consists of three fully connected hidden layers with 128, 128, and 64 nodes, respectively. Each hidden layer is integrated with a batch normalization layer to stabilize training and a dropout layer (rate of 0.3) to facilitate epistemic uncertainty estimation. These dropout layers remain active during inference to allow for stochastic sampling of the network weights.
- **Training and Optimization:** The network is trained for a maximum of 2000 epochs with an early stopping patience of 50 iterations. We apply a weight decay of  $1 \times 10^{-6}$  and utilize a learning rate of 0.001 with a

batch size depending on the dataset scale, fixing 32 for small samples (less than 10000), 120 for larger datasets (above 10000), and 250 specifically for the *WEC* benchmark.

- **Envelope Construction:** To construct the credal envelope, we utilize Monte Carlo Dropout to generate  $N_{MC} = 1000$  samples from the posterior distribution of the quantiles. By maintaining stochastic dropout at test time, we obtain a distribution of quantile estimates that reflects the inherent model ambiguity. For a given test point  $x$ , the credal envelope  $[\underline{C}(x), \overline{C}(x)]$  is derived by computing the  $\gamma(x)/2$  and  $1 - \gamma(x)/2$  quantiles of these MC samples, respectively. This procedure ensures that the envelope boundaries are directly informed by the epistemic uncertainty captured within the model’s posterior, allowing the prediction intervals to adapt to regions of high ambiguity.

## C.2 Adaptive Gamma standard parameter choices

The width of the credal envelope in CREDO is determined by the parameter  $\gamma$ , which dictates which quantiles are extracted from the model’s posterior distribution to represent model ambiguity. While  $\gamma$  can be a fixed global hyperparameter, our framework features an adaptive scheme that scales  $\gamma(x)$  based on the local geometry of the feature space. This configuration utilizes the scarcity score  $sc(x)$  defined in Eq. (4).

To maintain statistical consistency across varying geometries, we employ a heuristic for the number of neighbors  $k$  that accounts for the training sample size  $n$  and input dimensionality  $d$  [Zhao and Lai, 2022]:

$$k = \lceil C_{base} \cdot n^{\frac{4}{4+d}} \rceil$$

where  $C_{base} = 6.672$ . This formulation ensures that  $k$  scales at an optimal rate to balance bias and variance, preventing the scarcity metric from collapsing in high-dimensional spaces. The scarcity score is mapped to  $\gamma(x)$  to dictate the "credalness" of the prediction, constrained by the defaults  $\gamma_{min} = 0.1$  and  $\gamma_{max} = 0.75$ .

These thresholds are specifically chosen to balance the tradeoff between informativeness and the potential saturation of the envelopes in practice. Specifically,  $\gamma_{max}$  establishes the baseline for epistemic uncertainty in high-density regions, ensuring the envelope maintains a minimum informative width and does not collapse into a single point. Conversely,  $\gamma_{min}$  acts as a lower bound for the quantile levels in sparse regions; by reaching this limit, the envelope expands to capture the extreme tails of the posterior without becoming non-informative or excessively wide.

Additionally, by default, we set the scarcity threshold  $m_\gamma = 0$  and the scaling parameter  $\tau_\gamma = 1$ . To ensure the robustness of the mapping, we incorporate a small numerical constant  $\epsilon = 1 \times 10^{-6}$  within the scarcity calculations, providing stability in highly clustered regions of the feature space. Furthermore, the representation  $\phi(x)$  is defined as the standardized features to maintain a consistent scale across different datasets.

## C.3 BART-Based Credal Envelope

As a non-parametric alternative to neural architectures, we leverage Bayesian Additive Regression Trees (BART) to derive the credal envelope. While BART provides a more formal Bayesian posterior compared to dropout-based approximations, it was primarily utilized in our toy examples and illustrations. Due to the high computational cost of MCMC sampling, the Quantile Neural Network (QNN) architecture was preferred for the real-world benchmarks, as it offered better scalability without sacrificing predictive performance.

- **Model Specification:** We utilize a heteroscedastic formulation of BART, where both the conditional mean and the residual variance are modeled as functions of the covariates. Specifically, the model assumes  $Y = f(x) + \epsilon(x)$ , where  $f(x) = \sum_{j=1}^m T_j(x; M_j)$  is a sum of regression trees capturing the mean, and the noise term  $\epsilon(x) \sim \mathcal{N}(0, \sigma^2(x))$  follows a variance process also governed by a secondary tree ensemble. This allows the model to capture local variations in aleatoric noise while the Bayesian prior over the tree structures and leaf parameters accounts for epistemic uncertainty.
- **MCMC Sampling:** We employ Markov Chain Monte Carlo (MCMC) to generate samples from the posterior distribution of the regression function. These chains provide a rich, non-parametric representation of model ambiguity, as each iteration in the chain reflects a valid hypothesis for the underlying data-generating process given the evidence.
- **Envelope Construction:** For a test point  $x$ , we construct the credal envelope by leveraging the full posterior distribution captured through MCMC sampling. Specifically, we utilize the tree-based model structure

to generate a collection of quantile estimates from each iteration of the posterior chain. The final boundaries  $[\underline{C}(x), \overline{C}(x)]$  are then defined by extracting the empirical  $\gamma(x)/2$  and  $1 - \gamma(x)/2$  quantiles across this distribution of quantile estimates. This hierarchical approach ensures the envelope reflects the model's epistemic uncertainty by directly quantifying the variance among the different candidate models stored in the MCMC chains.

## D Proofs

**Lemma D.1** (Quantile sandwich). *Let  $Y \sim F$  where  $F$  is a CDF, and let  $q = F^{-1}(p)$  for  $p \in (0, 1)$ . Then*

$$\mathbb{P}(Y < q) \leq p \quad \text{and} \quad \mathbb{P}(Y \leq q) \geq p.$$

Consequently, for any  $0 < p < 1/2$ ,

$$\mathbb{P}(F^{-1}(p) \leq Y \leq F^{-1}(1-p)) \geq 1 - 2p.$$

*Proof.* By definition of  $q = F^{-1}(p)$ , we have  $F(t) < p$  for all  $t < q$  and  $F(q) \geq p$ . Thus  $\mathbb{P}(Y < q) = \sup_{t < q} \mathbb{P}(Y \leq t) = \sup_{t < q} F(t) \leq p$ . Also  $\mathbb{P}(Y \leq q) = F(q) \geq p$ . The last display follows by a union bound:

$$\mathbb{P}(Y < F^{-1}(p)) \leq p, \quad \mathbb{P}(Y > F^{-1}(1-p)) = 1 - \mathbb{P}(Y \leq F^{-1}(1-p)) \leq p.$$

□

*Proof of Theorem 3.1.* Fix  $x$  and  $F \in \mathcal{F}_0(x)$ , and define the  $F$ -central endpoints

$$q_L(F, x) := F^{-1}(\alpha_0/2 \mid x), \quad q_U(F, x) := F^{-1}(1 - \alpha_0/2 \mid x).$$

By definition of  $\ell(x)$  as an infimum over  $F$ -quantiles,  $\ell(x) \leq q_L(F, x)$ . By definition of  $u(x)$  as a supremum over  $F$ -quantiles,  $u(x) \geq q_U(F, x)$ . Hence

$$[\ell(x), u(x)] \supseteq [q_L(F, x), q_U(F, x)].$$

Applying Lemma D.1 conditionally on  $X = x$  gives

$$\mathbb{P}_F(q_L(F, x) \leq Y \leq q_U(F, x) \mid X = x) \geq 1 - \alpha_0.$$

Because  $[\ell(x), u(x)]$  contains  $[q_L(F, x), q_U(F, x)]$ , the same lower bound holds for  $[\ell(x), u(x)]$ . □

*Proof of Theorem 3.2.* By construction of  $C_L(x)$  and  $C_U(x)$ , we have

$$\pi(q_L(\theta, x) \leq C_L(x) \mid D_{\text{tr}}) = \gamma/2, \quad \pi(q_U(\theta, x) \geq C_U(x) \mid D_{\text{tr}}) = \gamma/2.$$

Hence

$$\pi(q_L(\theta, x) \geq C_L(x) \mid D_{\text{tr}}) \geq 1 - \gamma/2, \quad \pi(q_U(\theta, x) \leq C_U(x) \mid D_{\text{tr}}) \geq 1 - \gamma/2.$$

Let  $R_{qq}(x) = \{\theta : q_L(\theta, x) \geq C_L(x), q_U(\theta, x) \leq C_U(x)\}$ . By the union bound,

$$\pi(\theta \in R_{qq}(x) \mid D_{\text{tr}}) \geq 1 - \gamma.$$

Now fix any  $\theta \in R_{qq}(x)$ . Then  $[q_L(\theta, x), q_U(\theta, x)] \subseteq [C_L(x), C_U(x)] = [\ell(x), u(x)]$ , and therefore

$$\mathbb{P}_\theta(Y \in [\ell(x), u(x)] \mid X = x) \geq \mathbb{P}_\theta(Y \in [q_L(\theta, x), q_U(\theta, x)] \mid X = x).$$

The interval  $[q_L(\theta, x), q_U(\theta, x)]$  is the central  $(1 - \alpha_0)$  quantile interval under  $F_\theta(\cdot \mid x)$ , so it satisfies

$$\mathbb{P}_\theta(Y \in [q_L(\theta, x), q_U(\theta, x)] \mid X = x) \geq 1 - \alpha_0,$$

and thus, for all  $\theta \in R_{qq}(x)$ ,

$$\mathbb{P}_\theta(Y \in [\ell(x), u(x)] \mid X = x) \geq 1 - \alpha_0.$$

Finally, by the definition of the posterior predictive probability,

$$\begin{aligned}
\mathbb{P}(Y \in [\ell(x), u(x)] \mid X = x, D_{\text{tr}}) &= \int \mathbb{P}_{\theta}(Y \in [\ell(x), u(x)] \mid X = x) d\pi(\theta \mid D_{\text{tr}}) \\
&\geq \int_{R_{qq}(x)} \mathbb{P}_{\theta}(Y \in [\ell(x), u(x)] \mid X = x) d\pi(\theta \mid D_{\text{tr}}) \\
&\geq (1 - \alpha_0) \pi(\theta \in R_{qq}(x) \mid D_{\text{tr}}) \\
&\geq (1 - \alpha_0)(1 - \gamma),
\end{aligned}$$

which proves the claim.  $\square$

*Proof of Theorem 3.3.* Follows from the standard split-conformal arguments Vovk et al. [2005], Lei et al. [2018], Vovk et al. [2022], Izbicki [2025].  $\square$

**Assumption D.2** (Correct specification and posterior consistency). Let  $\alpha_0 = \alpha \in (0, 1)$ . Assume there exists a unique true parameter  $\theta^* \in \Theta$  such that the data are generated i.i.d. from the joint distribution induced by  $\theta^*$ , i.e.  $(X_i, Y_i)_{i \geq 1}$  are i.i.d. and for  $P_X$ -almost every  $x$ ,

$$Y \mid X = x \sim F_{\theta^*}(\cdot \mid x).$$

Let  $D_{\text{tr}}$  and  $D_{\text{cal}}$  be obtained by sample splitting with  $|D_{\text{tr}}| = n_{\text{tr}} \rightarrow \infty$  and  $|D_{\text{cal}}| = m \rightarrow \infty$ . All limits below are with respect to the joint draw of the full dataset (and, if applicable, the random split).

We assume:

(A1) **Posterior consistency for  $\theta$  (in probability)**. There exists a metric  $d$  on  $\Theta$  such that for every  $\varepsilon > 0$ ,

$$\pi(d(\theta, \theta^*) > \varepsilon \mid D_{\text{tr}}) \xrightarrow{\mathbb{P}_{\theta^*}} 0.$$

(A2) **Continuity of the endpoint functionals at  $\theta^*$** . For  $P_X$ -almost every  $x$ , define the endpoint maps (at nominal level  $\alpha$ )

$$q_L(\theta, x) = F_{\theta}^{-1}(\alpha/2 \mid x), \quad q_U(\theta, x) = F_{\theta}^{-1}(1 - \alpha/2 \mid x).$$

Assume  $q_L(\theta, x)$  and  $q_U(\theta, x)$  are continuous in  $\theta$  at  $\theta^*$  with respect to  $d$ .

(A3) **Regularity of the true conditional distribution at the oracle endpoints**. For  $P_X$ -almost every  $x$ , let

$$q_L^*(x) = F_{\theta^*}^{-1}(\alpha/2 \mid x), \quad q_U^*(x) = F_{\theta^*}^{-1}(1 - \alpha/2 \mid x).$$

Assume that  $F_{\theta^*}(\cdot \mid x)$  is continuous and strictly increasing in a neighborhood of  $q_L^*(x)$  and  $q_U^*(x)$  (equivalently, no atoms at the endpoints and no flat spots locally).

*Proof of Theorem 3.4. Step 1: posterior concentration transfers to the endpoints.* Fix  $\delta > 0$ . By continuity of  $q_L(\theta, x)$  at  $\theta^*$  (Assumption D.2(A2)), there exists  $\varepsilon(\delta) > 0$  such that  $d(\theta, \theta^*) \leq \varepsilon(\delta)$  implies  $|q_L(\theta, x) - q_L^*(x)| \leq \delta$ . Therefore,

$$\left\{ \theta : |q_L(\theta, x) - q_L^*(x)| > \delta \right\} \subseteq \left\{ \theta : d(\theta, \theta^*) > \varepsilon(\delta) \right\}.$$

Taking posterior probabilities conditional on  $D_{\text{tr}}$  gives

$$\pi(|q_L(\theta, x) - q_L^*(x)| > \delta \mid D_{\text{tr}}) \leq \pi(d(\theta, \theta^*) > \varepsilon(\delta) \mid D_{\text{tr}}).$$

By posterior consistency (Assumption D.2(A1)), the right-hand side converges to 0 in  $\mathbb{P}_{\theta^*}$ -probability, hence

$$\pi(|q_L(\theta, x) - q_L^*(x)| > \delta \mid D_{\text{tr}}) \xrightarrow{\mathbb{P}_{\theta^*}} 0. \quad (5)$$

The same argument yields

$$\pi(|q_U(\theta, x) - q_U^*(x)| > \delta \mid D_{\text{tr}}) \xrightarrow{\mathbb{P}_{\theta^*}} 0. \quad (6)$$

**Step 2: posterior quantiles of concentrated random variables converge.** We show  $\ell(x) = C_L(x) \rightarrow q_L^*(x)$  in probability; the proof for  $u(x)$  is identical. Let  $Z = q_L(\theta, x)$  under  $\theta \sim \pi(\cdot | D_{\text{tr}})$ , and let  $C_L(x)$  be its  $(\gamma(x)/2)$ -quantile under that posterior. Fix  $\delta > 0$ . If the posterior puts at least  $1 - \eta$  mass on the interval  $[q_L^*(x) - \delta, q_L^*(x) + \delta]$  for some  $\eta < \gamma(x)/2$ , then necessarily the  $(\gamma(x)/2)$ -quantile lies inside that interval, i.e.  $|C_L(x) - q_L^*(x)| \leq \delta$ . Formally, on the event

$$E_{\delta, \eta} := \{\pi(|Z - q_L^*(x)| \leq \delta | D_{\text{tr}}) \geq 1 - \eta\}, \quad \text{with } \eta < \gamma(x)/2,$$

we have  $\pi(Z \leq q_L^*(x) - \delta | D_{\text{tr}}) \leq \eta < \gamma(x)/2$ , so the  $(\gamma(x)/2)$ -quantile cannot be smaller than  $q_L^*(x) - \delta$ . Similarly,  $\pi(Z \leq q_L^*(x) + \delta | D_{\text{tr}}) \geq 1 - \eta > \gamma(x)/2$ , so the quantile cannot exceed  $q_L^*(x) + \delta$ . Hence, on  $E_{\delta, \eta}$  we have  $|C_L(x) - q_L^*(x)| \leq \delta$ .

By (5), for any fixed  $\eta > 0$ ,

$$\pi(|Z - q_L^*(x)| \leq \delta | D_{\text{tr}}) = 1 - \pi(|Z - q_L^*(x)| > \delta | D_{\text{tr}}) \xrightarrow{\mathbb{P}_{\theta^*}} 1,$$

so  $\mathbb{P}_{\theta^*}(E_{\delta, \eta}) \rightarrow 1$ . Therefore,  $\mathbb{P}_{\theta^*}(|\ell(x) - q_L^*(x)| > \delta) \rightarrow 0$ , i.e.  $\ell(x) \rightarrow q_L^*(x)$  in  $\mathbb{P}_{\theta^*}$ -probability. Repeating the same argument with (6) yields  $u(x) \rightarrow q_U^*(x)$ , proving (i).

**Step 3:  $\hat{\tau} \rightarrow 0$ .** Let  $(X, Y)$  denote an independent draw from the true distribution  $\mathbb{P}_{\theta^*}$ , independent of  $D_{\text{tr}}$ . Define the *oracle* interval and score as

$$I^*(X) := [q_L^*(X), q_U^*(X)] \text{ and } s^*(X, Y) := d(Y, I^*(X)),$$

and the learned score (based on  $D_{\text{tr}}$  only) as

$$s(X, Y) := d(Y, [\ell(X), u(X)]).$$

**(a) The oracle score has  $(1 - \alpha)$ -quantile equal to 0.** Fix  $\varepsilon > 0$ . By Assumption D.2(A3), for every  $x$ , the map  $t \mapsto F_{\theta^*}(t | x)$  is continuous and strictly increasing in a neighborhood of  $q_L^*(x)$  and  $q_U^*(x)$ . Therefore expanding the oracle interval by  $\varepsilon$  increases its conditional probability strictly:

$$\mathbb{P}_{\theta^*}(s^*(X, Y) \leq \varepsilon | X = x) = \mathbb{P}_{\theta^*}(Y \in [q_L^*(x) - \varepsilon, q_U^*(x) + \varepsilon] | X = x) > 1 - \alpha.$$

Taking expectation over  $X$  yields

$$p^*(\varepsilon) := \mathbb{P}_{\theta^*}(s^*(X, Y) \leq \varepsilon) = \mathbb{E}[\mathbb{P}_{\theta^*}(s^*(X, Y) \leq \varepsilon | X)] > 1 - \alpha. \quad (7)$$

**(b) The learned score converges to the oracle score.** Let  $(X, Y) \sim \mathbb{P}_{\theta^*}$  be independent of  $D_{\text{tr}}$ . By part (i), for every  $\delta > 0$  we have, for  $P_X$ -a.e.  $x$ ,  $\mathbb{P}_{\theta^*}(|\ell(x) - q_L^*(x)| > \delta) \rightarrow 0$  and  $\mathbb{P}_{\theta^*}(|u(x) - q_U^*(x)| > \delta) \rightarrow 0$ . Since these probabilities are bounded by 1, dominated convergence implies

$$\mathbb{P}_{\theta^*}(|\ell(X) - q_L^*(X)| > \delta) = \int \mathbb{P}_{\theta^*}(|\ell(x) - q_L^*(x)| > \delta) dP_X(x) \rightarrow 0,$$

and similarly  $\mathbb{P}_{\theta^*}(|u(X) - q_U^*(X)| > \delta) \rightarrow 0$ . Thus  $\ell(X) \rightarrow q_L^*(X)$  and  $u(X) \rightarrow q_U^*(X)$  in  $\mathbb{P}_{\theta^*}$ -probability. Moreover, for any  $y$  and any intervals  $[a, b]$  and  $[a', b']$ ,

$$|d(y, [a, b]) - d(y, [a', b'])| \leq |a - a'| + |b - b'|.$$

Applying this with  $a = \ell(X)$ ,  $b = u(X)$ ,  $a' = q_L^*(X)$ , and  $b' = q_U^*(X)$  yields

$$|s(X, Y) - s^*(X, Y)| \leq |\ell(X) - q_L^*(X)| + |u(X) - q_U^*(X)| \xrightarrow{\mathbb{P}_{\theta^*}} 0.$$

Therefore

$$s(X, Y) \xrightarrow{\mathbb{P}_{\theta^*}} s^*(X, Y). \quad (8)$$

**(c) The conditional score CDF at  $\varepsilon$  exceeds  $1 - \alpha$  with high probability.** Fix  $\varepsilon > 0$  and set  $\varepsilon' = \varepsilon/2$ . On the event  $\{|s(X, Y) - s^*(X, Y)| \leq \varepsilon'\}$ , the inclusion  $\{s^*(X, Y) \leq \varepsilon'\} \subseteq \{s(X, Y) \leq \varepsilon\}$  holds, hence

$$\mathbb{P}_{\theta^*}(s(X, Y) \leq \varepsilon | D_{\text{tr}}) \geq \mathbb{P}_{\theta^*}(s^*(X, Y) \leq \varepsilon') - \mathbb{P}_{\theta^*}(|s(X, Y) - s^*(X, Y)| > \varepsilon' | D_{\text{tr}}).$$

By (7), the first term equals  $p^*(\varepsilon') > 1 - \alpha$ . By (8) and Markov's inequality,

$$\mathbb{P}_{\theta^*}(|s(X, Y) - s^*(X, Y)| > \varepsilon' \mid D_{\text{tr}}) \xrightarrow{\mathbb{P}_{\theta^*}} 0.$$

Therefore,

$$\mathbb{P}_{\theta^*}(s(X, Y) \leq \varepsilon \mid D_{\text{tr}}) > 1 - \alpha \quad \text{with probability tending to 1.} \quad (9)$$

**(d) Conclude  $\hat{\tau} \rightarrow 0$ .** Let  $s_1, \dots, s_m$  be the calibration scores and define  $\hat{F}_m(t) = \frac{1}{m} \sum_{i=1}^m \mathbb{I}\{s_i \leq t\}$ . Conditional on  $D_{\text{tr}}$ , the  $s_i$ 's are i.i.d., so by the weak law, for any  $\eta > 0$ ,

$$\hat{F}_m(\varepsilon) - \mathbb{P}_{\theta^*}(s(X, Y) \leq \varepsilon \mid D_{\text{tr}}) \xrightarrow{\mathbb{P}_{\theta^*}} 0 \quad \text{as } m \rightarrow \infty.$$

Combine this with (9). Since  $k = \lceil (m+1)(1-\alpha) \rceil$  satisfies  $(k-1)/m \rightarrow 1 - \alpha$ , the event  $\{\hat{F}_m(\varepsilon) > (k-1)/m\}$  holds with probability tending to 1, and on this event at least  $k$  scores are  $\leq \varepsilon$ , implying the  $k$ -th order statistic satisfies  $\hat{\tau} \leq \varepsilon$ . Thus for every  $\varepsilon > 0$ ,

$$\mathbb{P}_{\theta^*}(\hat{\tau} > \varepsilon) \rightarrow 0,$$

i.e.  $\hat{\tau} \xrightarrow{\mathbb{P}_{\theta^*}} 0$ .

**Step 4: conditional coverage converges to  $1 - \alpha$ .** Fix  $x$ . The conditional coverage of the final interval is

$$\mathbb{P}_{\theta^*}(Y \in C(x) \mid X = x, D_{\text{tr}}, D_{\text{cal}}) = F_{\theta^*}(u(x) + \hat{\tau} \mid x) - F_{\theta^*}(\ell(x) - \hat{\tau} \mid x),$$

using continuity of  $F_{\theta^*}(\cdot \mid x)$  (Assumption D.2(A3)). By (i) and (ii) and Slutsky's theorem,

$$(\ell(x) - \hat{\tau}, u(x) + \hat{\tau}) \xrightarrow{\mathbb{P}_{\theta^*}} (q_L^*(x), q_U^*(x)).$$

Because  $F_{\theta^*}(\cdot \mid x)$  is continuous, the map  $(a, b) \mapsto F_{\theta^*}(b \mid x) - F_{\theta^*}(a \mid x)$  is continuous, so by the continuous mapping theorem,

$$F_{\theta^*}(u(x) + \hat{\tau} \mid x) - F_{\theta^*}(\ell(x) - \hat{\tau} \mid x) \xrightarrow{\mathbb{P}_{\theta^*}} F_{\theta^*}(q_U^*(x) \mid x) - F_{\theta^*}(q_L^*(x) \mid x).$$

Finally, since  $q_L^*(x)$  and  $q_U^*(x)$  are the  $\alpha/2$  and  $1 - \alpha/2$  quantiles and the CDF is continuous at these points,  $F_{\theta^*}(q_L^*(x) \mid x) = \alpha/2$  and  $F_{\theta^*}(q_U^*(x) \mid x) = 1 - \alpha/2$ , hence the limit is  $1 - \alpha$ . This proves (iii).  $\square$